

ESD-TDR-64-25

~~ESTI PROCESSED~~☐ DDC TAB ☐ PROJ OFFICER☐ ACQUISITION MASTER FILE☐ _____

DATE _____

ESTI CONTROL NR. AL-40295CY NR. 1 OF 1 CYS

ESD RECORD COPY

RETURN TO
SCIENTIFIC & TECHNICAL INFORMATION DIVISION
(ESTI), BUILDING 1211

COPY NR. _____ OF _____ COPIES

Technical Report

345

Interpretation
of the
Magnetic and Crystallographic
Properties of Compounds
with the B31 Structure

J. B. Goodenough

28 January 1964

Prepared under Electronic Systems Division Contract AF 19(628)-500 by

Lincoln Laboratory

MASSACHUSETTS INSTITUTE OF TECHNOLOGY

Lexington, Massachusetts



AD0435758

The work reported in this document was performed at Lincoln Laboratory, a center for research operated by Massachusetts Institute of Technology, with the support of the U.S. Air Force under Contract AF 19(628)-500.

Non-Lincoln Recipients

PLEASE DO NOT RETURN

Permission is given to destroy this document
when it is no longer needed.

MASSACHUSETTS INSTITUTE OF TECHNOLOGY
LINCOLN LABORATORY

INTERPRETATION OF THE MAGNETIC
AND CRYSTALLOGRAPHIC PROPERTIES
OF COMPOUNDS WITH THE B31 STRUCTURE

J. B. GOODENOUGH

Group 82

TECHNICAL REPORT 345

28 JANUARY 1964

LEXINGTON

MASSACHUSETTS

ABSTRACT

The orthorhombic B31 structure, typified by MnP, is interpreted as a distortion of the hexagonal NiAs (B8₁) structure due to metal-metal bonding within the hexagonal basal planes. The number of d-like electrons per cation is known from the chemical formula provided the Fermi level lies in an energy gap between filled and empty bands of broad-band states, as is generally the case where there is a large electronegativity difference between cation and anion. It is argued that in stoichiometric materials, with an integral electron/cation ratio, it is possible to define operationally a critical cation-cation separation R_c such that the d-like states must be treated as collective states if $R < R_c$, may be treated as localized states if $R > R_c$. An empirical value for R_c is presented for transition-metal oxides. Since the cubic component of the ligand fields and the intra-atomic exchange give splittings that are larger than the widths of d-like bands, it is possible to construct schematic one-electron energy diagrams for various electron/cation ratios. From knowledge of R_c , it is possible to distinguish localized from collective d-like states that are simultaneously present. These diagrams are used to obtain the spin-only contribution to the atomic moment. For the case $R > R_c$, it is possible to derive interatomic spin correlations from the Heisenberg exchange Hamiltonian and superexchange theory. With the assumption that the sign of the cation-cation exchange couplings stay the same as R varies through R_c , it is possible to make sharp predictions of Pauli paramagnetism vs antiferromagnetism vs metamagnetism vs ferromagnetism as a function of electron/cation ratio. The low-temperature spin configuration of metamagnetic MnP is predicted to be a strongly distorted spiral propagating along the orthorhombic c-axis with spins lying mostly in the b-c plane. It is also noted that the B20 structure of FeSi can be interpreted as a distortion of the zinc-blende structure due to metal-metal bonding.

This technical documentary report is approved for distribution.

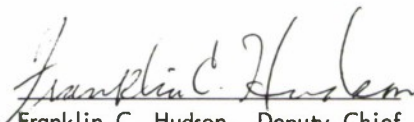

Franklin C. Hudson, Deputy Chief
Air Force Lincoln Laboratory Office

TABLE OF CONTENTS

Abstract	iii
I. INTRODUCTION	1
II. ESTIMATE OF R_c^{nl}	2
A. The Problem	2
B. Operational Parameters	2
C. An Empirical Expression for R_c^{3d} in Oxides	6
III. APPLICATION TO B31 COMPOUNDS	9
A. Construction of a Hamiltonian	9
B. The MnP (B31) Structure	11
C. Construction of Energy Diagrams	14
D. Magnetic Order and Atomic Moment	19
IV. CONCLUSIONS	22
APPENDIX A	25
APPENDIX B	27
APPENDIX C	28

INTERPRETATION OF THE MAGNETIC AND CRYSTALLOGRAPHIC PROPERTIES OF COMPOUNDS WITH THE B31 STRUCTURE

I. INTRODUCTION

A fundamental problem for solid state physics is an adequate description of narrow-band electrons, where by narrow is meant a bandwidth $\Delta\epsilon \lesssim 1$ ev. The problem is of intellectual importance, since there is need of a conceptual transition – aside from the purely formal inclusion of higher-order configurations in the expansion of a set of basis wave functions – from the plane-wave models of broad-band theory to the localized-electron models of ligand-field theory. It is also of practical importance since many transition-element compounds contain narrow-band electronic states. In order to study experimentally the properties of narrow-band electrons, it is preferable to have a compound or system in which the occupied narrow-band states lie in an energy gap between a filled valence band and an empty conduction band of broad-band states. The present study of MnP, which has the B31 structure, is an extension of this type of study from oxides^{1†} to compounds containing other anions. However, before the experimental results can be adequately interpreted, it is necessary to introduce the concept of a critical interatomic separation R_c for which the localized-electron assumption of ligand-field theory is adequate if $R > R_c$. Such a concept implies a fairly sharp transition with R in certain well-defined, operational parameters, so that it is subject to experimental verification. However, there appears to be an inherent lack of stability associated with $R \approx R_c$, which makes chemical preparation of a suitable system for the observation of R_c quite challenging! In Sec. II, some experimental data and physical arguments are advanced in support of a semi-empirical expression for the parameter R_c . In Sec. III, a general Hamiltonian is presented and applied to the construction of an energy-level diagram for MnP. The theory contains several parameters whose relative magnitudes can be estimated. One of these parameters, which is responsible for the relative energies of narrow-band states with differing interatomic spin correlations, is estimated from a simple extrapolation of superexchange theory, which defines the interatomic spin correlations for the localized-electron case. This extrapolation leads to predictions for the signs of the magnetic interactions in MnP that permit interpretation of the complex metamagnetic behavior of this compound. (The significance of this extrapolation procedure and the concept of an R_c is heightened by the fact that the postulates that have been previously presented² for correlating the magnetic, structural, and electronic-specific-heat data of the transition elements and their binary alloys follow immediately from them.) Finally, energy-level diagrams for other B31 compounds with different electron-atom ratios are presented, and definite

† References are listed on p. 35.

predictions about their magnetic properties are made. These predictions will be tested in future experimental work.

II. ESTIMATE OF R_c^{nl}

A. The Problem

From experiment it is clear that for large cation-cation separations the outer electrons on transition-metal cations can be adequately characterized as localized electrons that have the same symmetry properties as atomic d wave functions. This fact is the basis of ligand-field theory, which provides the energy-level splittings of these electronic states in terms of defined parameters whose magnitudes are best estimated from experiment. It is also evident from experiment that, at small cation-cation separations, electrons in states that are directed along the cation-cation bonds cannot be adequately described as localized electrons. The superconductors with A15 structure, such as Nb_3Sn , forcefully illustrate this fact. Therefore, there must be a transition in the character of the outer d electrons as the cation-cation separation R is changed. This poses the following questions: What operational parameters change significantly as R varies through the transition region? How sharp is the transition region?

B. Operational Parameters

There are four operational parameters that are chosen for discussion: paramagnetic susceptibility χ_m , the exchange parameter J_{ij}^{ex} , the electrical conductivity σ , and the local crystallographic symmetry about the cations.

1. Magnetic Susceptibility

In the localized-electron limit ($R > R_c$), χ_m is given by the Curie-Weiss law. In the limit $R \ll R_c$, χ_m is temperature independent (Pauli paramagnetism). As $R \rightarrow R_c^-$, the bandwidth $\Delta\epsilon$ decreases, so that higher-order terms of the Pauli paramagnetism expression become important, especially at higher temperatures. Therefore, the high-temperature χ_m should decrease relatively slowly with R for $R \leq R_c$. For $R > R_c$ and low temperatures, there is a spontaneous atomic moment and long-range magnetic coupling may occur to introduce either ferromagnetism or an anisotropic χ_m characteristic of antiferromagnetism. For $R > R_c$ and low temperatures, there is no spontaneous atomic moment and the weak paramagnetic susceptibility is nearly temperature independent. Therefore, low-temperature measurements of χ_m can provide an operational definition for R_c . However, if there are two types of partially filled electronic states, those with $R < R_c$ and those with $R > R_c$, that are simultaneously occupied, electrons in states with $R > R_c$ introduce a spontaneous atomic moment that dominates χ_m .

2. Magnetic Coupling

For $R > R_c$, the interatomic spin correlations are given by the ground-state spin configuration. It has been found that if the Heisenberg exchange Hamiltonian $H_{ex} = -\sum_{ij} J_{ij}^{ex} \vec{S}_i \cdot \vec{S}_j$, where \vec{S} is the total cation spin, is used, solutions of this many-body problem can usually be obtained that correspond to the observed spin configurations.³ Further, the strength of the exchange parameter J_{ij}^{ex} between neighboring atoms or ions with overlapping, localized (ligand-field) wave functions $\phi(\vec{r}_i)$, $\phi(\vec{r}_j)$ may be expressed⁴ as

$$\begin{aligned}
J_{ij} &= -b_{ij}^2/(2S^2U) && \text{if the overlapping orbitals each} \\
&&& \text{contain one electron,} \\
J_{ij} &= +b_{ij}^2 J^{\text{intra}}/(2S^2U^2) && \text{if the overlapping orbitals each} \\
&&& \text{contain an average of either one-} \\
&&& \text{half or three-halves electrons.}
\end{aligned} \tag{1}$$

where J^{intra} is the intra-atomic exchange energy, U is the electrostatic energy to be associated with an electron transfer, and b_{ij} is the one-electron transfer integral that appears in the tight-binding expression for the bandwidth $\Delta\epsilon$ of an orbitally nondegenerate band:

$$\epsilon_m(\vec{k}) = a_m + \sum_{\vec{\tau}} b_m(\vec{\tau}) \exp[-i\vec{k} \cdot \vec{\tau}] \quad . \tag{2}$$

The $\vec{\tau}$ are the fundamental (nonzero) translations of the lattice, so that

$$\Delta\epsilon = Cb(\vec{\tau}) \quad , \tag{3}$$

and $C \sim 10$ is a constant that depends upon the crystal structure. The perturbation theory leading to Eq. (1) breaks down as $R \rightarrow R_c^+$ since $U \rightarrow 0$ as $R \rightarrow R_c^+$ (see discussion on electrical conductivity in Sec. II-B-3), whereas the transfer integral increases continuously with decreasing R through R_c . Therefore, $J_{ij}^{\text{ex}}(R)$ should increase with decreasing R throughout the range $R > R_c$. The dependence of J_{ij}^{ex} on R for $R < R_c$ has not been formulated. It apparently goes through a maximum with decreasing R , since the magnetic coupling of the 4f electrons via broad-band electrons is relatively weak in the rare-earth metals. Therefore, the R -dependence of J_{ij}^{ex} can be assumed to be particularly strong in the neighborhood of $R \approx R_c$. Since thermal expansion makes R a function of temperature, the exchange parameter $J_{ij}^{\text{ex}} = J_{ij}^{\text{ex}}(T)$ is particularly sensitive to temperature if two conditions are met: (a) the thermal expansion coefficient is large, and (b) $R \approx R_c$. This conclusion is important because the internal fields of molecular-field theory, which are proportional to J_{ij}^{ex} , are assumed temperature-independent in conventional derivations of the Curie-Weiss law. If $J_{ij}^{\text{ex}} = \sum_n J_n T^n$ and the leading two terms are dominant, then χ_m has the form of the Curie-Weiss law but the Curie constant and paramagnetic Curie temperature have different interpretations. More spectacular, perhaps, are the magnetic order \rightleftharpoons order transitions that are induced by temperature-dependent exchange parameters. Magnetic order \rightleftharpoons order transitions may occur if one of two competitive exchange interactions is more temperature sensitive. Such a transition is illustrated by the metamagnetic \rightleftharpoons ferromagnetic transition recently found⁵ in MnP. From a knowledge of the types of magnetic order above and below the transition and a general theory for the magnetic order as a function of the exchange parameters, it is possible to determine which exchange interaction is the more temperature sensitive. This provides a direct test for the above assumption that the most temperature-sensitive interaction is a cation-cation interaction having $R \approx R_c$.

Since there is no theory for long-range interatomic spin correlations in the range $R = R_c - \delta R$, any empirical information that is relevant to this problem is important. The most direct experimental evidence is the magnetic order at low temperatures in those cases where localized ($R > R_c$) and collective ($R < R_c$) electrons are simultaneously present. For the rare-earth metals, for example, the 4f electrons are localized and the dominant interatomic coupling appears to be via the correlations between spin-density regions that they induce among the broad-band electrons. In the transition metals, there is ample evidence² that both localized and

collective d states may be partially filled simultaneously. (Theoretical justification for such a concept may be found in Nesbet's⁶ studies of diatomic molecules.) In such a case, it is possible to associate a definite spin with the anisotropic ligand-field function $\phi(\vec{r}_i)$ that is directed toward cation near neighbors at $R > R_c$. If the collective-electron d states that are directed along crystallographic directions having $R = R_c - \delta R$ are partially filled, the spin density from all collective electrons that is induced by the localized spins will be dominated by states having the highest density of states at the Fermi surface, or by the narrow-band states. (If the Fermi level lies in an energy gap between broad bands, only the narrow-band contribution is present.) It is reasonable to assume that for small δR , the sign of the J_{ij}^{ex} between cations having $R = R_c - \delta R$ is, in this case, the same as that predicted from Eq. (1), which applies to the case $R = R_c + \delta R$. (The Ruderman-Kittel-Kasuya-Yosida^{7,8} formalism applies only in the broad-band limit.) One of the objectives of the present experimental program is to determine whether this assumption does provide a reliable guide for predicting the signs of the magnetic couplings in transition-metal alloys.

3. Electrical Conductivity

The electrical conductivity is

$$\sigma = \sum_i n_i q_i \mu_i \quad , \quad (4)$$

where n_i is the density of carriers having charge q_i and mobility μ_i . For localized ($R > R_c$) d electrons, two cases must be distinguished: the intrinsic case, which corresponds to an integral number of d electrons per cation (e.g., Fe_2O_3), and the extrinsic case, which corresponds to a nonintegral number of d electrons per equivalent cation (e.g., Fe_3O_4), where by equivalent cation is meant cations of the same element on similar lattice sites. For the intrinsic case, the arguments of Mott⁹ for a sharp R_c apply. In this case, there are two types of d-electron carriers, electrons of density n and holes of density p . (The model used here is that given by Jonker.¹⁰) In this case, $n = p$ and

$$n = n_0 \exp[-\epsilon_g/2kT] \quad , \quad (5)$$

where ϵ_g is the energy required to create a separated hole-electron pair. Since

$$\epsilon_g \sim (e^2/\kappa r) \exp[-\sigma' r] \quad , \quad (6)$$

where σ' is the Mott screening parameter, which becomes much larger than R^{-1} for $R \rightarrow R_c^+$, a good operational definition for R_c is that value of interatomic separation R at which $\epsilon_g \rightarrow 0$ as $R \rightarrow R_c^+$. If $R > R_c$, the motion of the separated charge carriers is given by diffusion theory and

$$\mu_n = eD/kT \propto T^{-1} \exp[-\epsilon_a/kT] \quad , \quad (7)$$

where ϵ_a represents the activation energy for an electron to hop from one lattice site to the next.¹¹ Since the exponential temperature dependence overwhelms the T^{-1} dependence in the usual temperature interval of measurement, the electrical conductivity can be represented by the temperature dependence [from Eqs. (4), (5), (7)]

$$\sigma \approx \sigma_0 \exp[-q/kT] \quad , \quad q = (\epsilon_g/2) + \epsilon_a \quad , \quad (8)$$

provided the difference in activation energies for hole and electron hops is much less than kT . If ϵ_g is as sensitive a function of R in the region $R = R_c + \delta R$ as Eq. (6) suggests, then measurements of σ in intrinsic materials can provide a sharp operational definition for R_c even though the value of R at which ϵ_a vanishes may not be sharply defined. If the temperature dependence of the conductivity due to d-electron charge carriers is metallic, then $R < R_c$ as defined by both ϵ_g and ϵ_a .

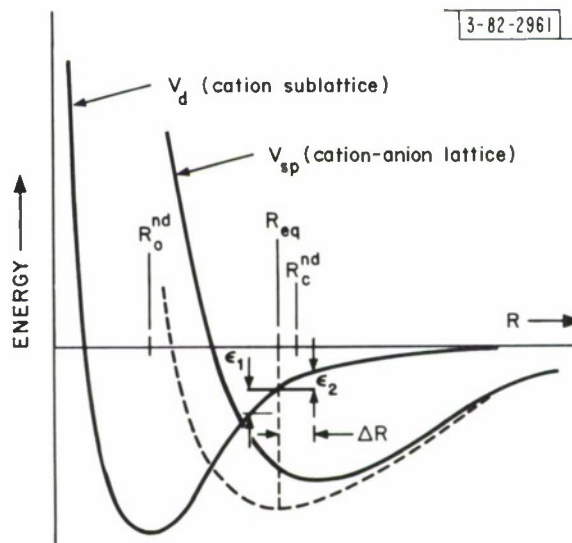
In order to apply this conductivity criterion with confidence, it is necessary to know whether the charge carriers in question are d-like carriers or are broad-band carriers. This question can generally be settled by a measure of the magnitude of the charge-carrier mobility (e.g., by a supplemental measurement of the Hall effect). Broad-band carriers have mobilities $\mu \sim 10^2 - 10^3 \text{ cm}^2/\text{v-sec}$, localized electrons have mobilities at room temperature $\mu < 1 \text{ cm}^2/\text{v-sec}$, and narrow-band electrons have room-temperature mobilities in the range $0.5 < \mu < 50 \text{ cm}^2/\text{v-sec}$. (See bottom of Table II.)

4. Local Cation Symmetry

The melting point T_{mp} of transition-metal compounds is determined primarily by the outer s and p electrons and the Madelung energy, d-electron bonding playing a secondary role. Therefore, ordering of the d electrons into a configuration that optimizes d-electron bonding may occur at a $T_t < T_{mp}$. Examples of this type of electron ordering are: (a) order \rightleftharpoons disorder of Fe^{2+} ions in the inverse spinel magnetite, $\text{Fe}^{3+}[\text{Fe}^{2+}\text{Fe}^{3+}]\text{O}_4$; (b) order \rightleftharpoons disorder of atomic spins in magnetic compounds; (c) superconducting \rightleftharpoons normal conducting in Nb_3Sn ; (d) Jahn-Teller ordering in Mn_3O_4 ; (e) spin-orbit ordering below T_N in CoO ; (f) cation-cation bonding in VO_2 or FeS ; (g) cation-anion bonding that leads to ferroelectricity in BaTiO_3 . Of all the types of ordering that can be considered, only those involving cation-cation bonding give rise to a local cation symmetry in which the cation is moved away from the center of symmetry of its anion interstice toward a nearest-neighbor cation. Figure 1 is a schematic diagram of the electron potential energies V_{sp} and V_d vs interatomic spacing R for outer s and p and outer d electrons in a crystal with close-packed anion sublattice. For the case shown, the minimum in the composite curve occurs at an equilibrium separation $R_{eq} = R_c^{nd} - \delta R$, where the curvature

Fig. 1. Schematic electron potentials vs lattice parameter, expressed as a cation-cation separation R , for transition metals with a close-packed anion sublattice. Instabilities with respect to distortion from close-packed anion symmetry are not indicated.

$$\begin{aligned}\epsilon_1 &\approx \Delta R (dV_d/dR)_{R_{eq}} - \Delta R, \\ \epsilon_2 &\approx \Delta R (dV_d/dR)_{R_{eq}} + \Delta R.\end{aligned}$$



of $V_d(R)$ is negative. Although such a system is stable for simple dilation and contraction of the lattice, it is unstable to small distortions from close-packed anion symmetry that are induced by a shortening of some cation-cation distances, a lengthening of others. The change in d-electron binding energy due to such a distortion is

$$\Delta E_{\text{bind}} \approx \left\{ \left(\frac{dV_d}{dR} \right)_{R_{\text{eq}} + \Delta R} - \alpha \left(\frac{dV_d}{dR} \right)_{R_{\text{eq}} - \Delta R} \right\} \Delta R = -A_B \Delta R \quad (9)$$

if the number of bonds that are lengthened equals the number that are shortened. The parameter $\alpha \gtrsim 1$ is a measure of any correlation stabilization of $V_d(R)$ due to a change in the number of metal-metal nearest neighbors. A distortion from close-packed anion symmetry requires work against the elastic forces:

$$\Delta E_{\text{el}} = A_{\text{el}} (\Delta R)^2, \quad (10)$$

so that a distortion from close-packed anion symmetry that has

$$\Delta R = A_B / 2A_{\text{el}} \quad (11)$$

will lower the internal energy. The total change of internal energy per mole is

$$(\Delta S + Nk) T_t \approx (\Delta E_{\text{bind}} + \Delta E_{\text{el}}) = -\frac{1}{2} A_B \Delta R = -A_B^2 / 4A_{\text{el}} \quad (12)$$

where ΔS is the change in entropy due to the distortion. If $R \gg R_c$, A_B is too small to support a ΔR that is larger than the thermal vibrational amplitudes, and there is no static distortion unless it accompanies a magnetic ordering, in which case it appears as exchange striction. As $R \rightarrow R_{\text{eq}}^{\text{nd}}$, the curvature of $V_d(R)$ changes from negative to positive, and ΔR vanishes. Therefore only in the range $R = R_c \pm \delta R$ are static distortions due to cation-cation bonding likely to occur, and the presence of local cation symmetry indicative of cation-cation bonding will suggest a $\Delta R > \delta R$, or a distortion that reflects $R < R_c$ along the cation-cation bonds and $R > R_c$ where the cation-cation separation has been increased.

It should be noted that for large ΔR , it is possible to have $T_t = T_{\text{mp}}$, so that no cation-cation bonding transition is observed below the melting point. Also, if close-packed anion symmetry results in a cation ground state that has orbital degeneracy, a distortion involving cation-cation bonding removes this degeneracy and the parameter A_B may be particularly large.

C. An Empirical Expression for R_c^{3d} in Oxides

It is clear that any critical separation R_c^{nl} for equivalent electrons must depend upon at least three factors: the amount of s and p character admixed into the d-like wave functions, the contraction of the wave functions with increasing nuclear charge at the cation, and the intra-atomic exchange, which would induce localization of a net atomic moment at each cation. The first of these will make any R_c dependent upon the anion component. But for a given anion sublattice, the critical separation should be of the form

$$R_c^{3d} \approx \{ R_1 - R_2(Z - Z_{\text{Ti}}) - R_3 \Delta [J(J + 1)] \} \quad (13)$$

where R_1 is approximately constant for cations of similar formal valence, and Z_{Ti} and Z are the atomic numbers of Ti and of the first-row transition element in question. The distance R_2

can be estimated from a knowledge of ionic radii. From empirical ionic radii as discussed by Van Santen and Van Wieringen,¹² it is estimated that

$$R_2 \approx 0.03 \text{ \AA} \quad . \quad (14)$$

Given operational definitions for R_c , it is possible to turn to the sesquioxides Ti_2O_3 , V_2O_3 , Cr_2O_3 and $\alpha\text{Fe}_2\text{O}_3$, all of which have the corundum structure, to obtain empirical expressions for R_1 and R_3 in a close-packed oxygen sublattice.

In corundum the cations are in nearly octahedral interstices. Isolated pairs of cations along the c-axis share common octahedral-site faces and are separated by a distance R_{tt}^c . Within the basal planes each cation has three near-neighbor cations at a distance R_{tt}^b that share common octahedral-site edges. Only those d-like electrons occupying states with t_{2g} symmetry (d_{yz} , d_{zx} , d_{xy} if cation-anion bonds of ideal octahedral site define Cartesian axes) overlap directly the orbitals of neighboring cations. Now if $R_{tt}^c < R_{tt}^b < R_c^{3d}$, then any t_{2g} electrons occupy collective-electron, cation-sublattice states. Further, if this band of states is only partially occupied, then metallic conductivity should be observed, but with an intermediate charge-carrier mobility ($\mu \sim 1\text{-}10 \text{ cm}^2/\text{v-sec}$) characteristic of a narrow band. (Since there is a large electro-negativity difference between oxygen and the transition-metal atoms, it seems safe to assume that the broad-band electrons do not contribute appreciably to the conductivity, the Fermi level falling in an energy gap between valence and conduction bands.) If, on the other hand, $R_{tt}^b > R_c^{3d}$, then metallic conductivity is not possible even if $R_{tt}^c < R_c^{3d}$ because the c-axis pairs are isolated.

The critical experimental findings for the sesquioxides mentioned above have been discussed in an earlier publication.¹ The first important fact is that at high temperatures, stoichiometric V_2O_3 is metallic and Ti_2O_3 exhibits only a small activation energy, whereas Cr_2O_3 and $\alpha\text{-Fe}_2\text{O}_3$ are insulators. It might be argued that the t_{2g} bands are split in two by crystal symmetry, so that Cr_2O_3 and $\alpha\text{-Fe}_2\text{O}_3$ with three t_{2g} electrons have just filled the lower t_{2g} band, whereas this band is only partially filled in Ti_2O_3 and V_2O_3 . However, the activation energies of Cr_2O_3 and $\alpha\text{-Fe}_2\text{O}_3$ are too large for such an interpretation to be adequate. The second fact is that in Cr_2O_3 and $\alpha\text{-Fe}_2\text{O}_3$ the atomic moments are large, which implies localized electrons and splitting of the t_{2g} states by intra-atomic exchange. The susceptibilities of Ti_2O_3 and V_2O_3 do not obey a Curie-Weiss law and they exhibit a small, nearly isotropic, temperature-independent χ_m below an "apparent" Néel temperature. Therefore, it is concluded that $R_{tt}^b > R_c$ in Cr_2O_3 and $\alpha\text{-Fe}_2\text{O}_3$, but $R_{tt}^b \lesssim R_c$ in Ti_2O_3 and V_2O_3 . The room-temperature cation-cation separations are given in Table I. These distances are compatible with a critical distance at room temperature

$$R_c^{3d}(\text{oxides}) \approx \{ 3.02 - 0.03(Z - Z_{Ti}) - 0.04\Delta [J(J + 1)] \} \text{ \AA} \quad , \quad (15)$$

provided there is evidence that $R_{tt}^c(\text{Cr}) = 2.65 \text{ \AA} < R_c^{3d}(\text{Cr})$. Anomalous antiferromagnetic-resonance data,¹³ a rounded χ_m vs T curve at T_N ,¹⁴ and a reduced low-temperature atomic moment¹⁵ in Cr_2O_3 together with a fast relaxation of excited states in isolated $\text{Cr}^{3+} - \text{Cr}^{3+}$ pairs in chromium-substituted Al_2O_3 (Ref. 16) and color changes in the system $\text{Al}_2\text{O}_3 - \text{Cr}_2\text{O}_3$ (Ref. 17) all demonstrate an anomalously large ratio for the exchange coupling between c-axis to basal-plane neighbors,¹⁸ which is indicative of $R_{tt}^c(\text{Cr}) < R_c^{3d}$.

A recent neutron-diffraction study¹⁹ indicates that low-temperature Ti_2O_3 is antiferromagnetic with a titanium atomic moment $\mu_{Ti} \approx 0.2 \mu_B$. Were $R_{tt}^c(\text{Ti}) = 2.59 \text{ \AA} \ll R_c$ and the narrow Γ_{T1} band split by crystalline fields from the $\Gamma_{T3}^{1,2}$ states (trigonal symmetry stabilizes

TABLE I CATION-CATION DISTANCES IN ANGSTROM UNITS FOR FOUR OXIDES WITH CORUNDUM STRUCTURE, AS GIVEN BY REF. 22				
	Ti ₂ O ₃	V ₂ O ₃	Cr ₂ O ₃	α-Fe ₂ O ₃
R_{tt}^c	2.59	2.70	2.65	2.89
R_{tt}^b	2.99	2.88	2.89	2.97

a c-axis directed Γ_{T1} relative to basal-plane directed $\Gamma_{T3}^1, \Gamma_{T3}^2$ states among the three orbitals of t_{2g} symmetry), as was suggested previously,¹ the single Γ_{T1} electrons would form homopolar bonds and there should be no long-range magnetic order. In an alternate proposal,²⁰ the titanium electrons were assumed to be localized, and the semiconducting \rightarrow nearly metallic transition in Ti₂O₃ was claimed to reflect a splitting of the bands below T_N as a result of the magnetic order. Although the observed antiferromagnetic order of Ti₂O₃ is compatible with this proposal and the low moment can be attributed qualitatively to a large orbital-momentum contribution to the total angular-momentum quantum number $J = L - S$, the anomalous behavior of χ_m (Ref. 21) and the very low activation energy in the high-temperature conductivity of stoichiometric Ti₂O₃ argues for $R_{tt}^b \lesssim R_c$. Examination of the temperature dependence of R_{tt}^b is instructive:²² At 350°C > T_N , $R_{tt}^b = 2.96 \text{ \AA}$ and there is an increase in R_{tt}^b with decreasing temperature as the temperature is lowered through the broad temperature interval over which magnetic ordering takes place. Thus the high-temperature conductivity, which indicates $R_{tt}^b(\text{Ti}) < R_c^{\text{Ti}}$ is compatible with $R_{tt}^b(\text{Ti}) = 2.99 \text{ \AA} \gtrsim R_c^{\text{Ti}}$ at room temperature.

It should be noted that the two proposals for Ti₂O₃ are not so different as they at first appear. For $R = R_c - \delta R$ and antiferromagnetic coupling, strongly coupled antiparallel moments tend to be reduced below the ordering temperature, thus giving rise to a discontinuous decrease in χ_m as the temperature is lowered through T_N . The anomalous decrease in χ_m as T is lowered through T_N , and this in spite of an increasing R_{tt}^b , suggests that the spins of the Γ_{T1} component tend to cancel [$R_{tt}^c(\text{Ti}) < R_c^{\text{Ti}}$] and the observed moment is primarily due to the $\Gamma_{T3}^{1,2}$ component of the wave functions. In this case, the orbital-momentum contribution to the net moment can be considerably less than $0.8 \mu_B$, which is more reasonable since the ligand fields tend to quench it.

Finally, it should be noted that in metallic, hexagonal titanium, which is Pauli paramagnetic, $R_{tt}^b = 2.95 \text{ \AA} < R_c^{\text{Ti}}(\text{metal})$, which is further evidence that $R_{tt}^c(\text{Ti}) = 2.59 \text{ \AA} < R_c^{\text{Ti}}(\text{oxide})$ even though $R_c^{\text{Ti}}(\text{metal}) > R_c^{\text{Ti}}(\text{oxide})$ can be anticipated. If $R_{tt}^c(\text{Ti}) < R_c^{\text{Ti}}$ in Ti₂O₃ and ligand fields have removed any ground-state orbital degeneracy, then the observed long-range order, which has antiparallel c-axis pairs, indicates that if each overlapping orbital contains one electron, $J_{ij}^{\text{ex}} < 0$ as is predicted by an extrapolation of predictions from Eq. (1) to the region $R < R_c$.

Further evidence that $R_c^{3d}(\text{oxides})$ is well defined and well approximated by Eq. (15) comes from a study²³ of the electrical conductivity of a series of stoichiometric, normal vanadium spinels $M^{2+}[\text{V}_2^{3+}]\text{O}_4$, where $M = \text{Mn, Fe, Mg, Zn, Co}$. In this series, the activation energy q of

Eq. (8) was found to decrease regularly with R from $q = 0.37$ ev at $R_{tt}^V = 3.013 \text{ \AA}$ in $\text{Mn}[\text{V}_2]\text{O}_4$ to $q = 0.07$ ev at $R_{tt}^V = 2.972 \text{ \AA}$ in $\text{Co}[\text{V}_2]\text{O}$. These studies indicate an $R_c^V(\text{oxides}) \approx 2.95 \text{ \AA}$. (Metallic VO has a V-V separation of 2.894 \AA , which also indicates that R_c is quite sharply defined, the complete transition from semiconductor to metallic properties occurring within 0.1 \AA .)

Additional arguments in support of Eq. (15) are outlined in Appendix A.

III. APPLICATION TO B31 COMPOUNDS

A. Construction of a Hamiltonian

It will be assumed that in the B31 compounds the electronegativity difference between cations and anions is sufficiently large that the Fermi level lies in an energy gap between broad-band states. Therefore, only states belonging to a d-like manifold are considered, and the number of d-like electrons per metal atom are immediately given. Although there may be some overlap of broad-band and narrow-band states, especially in compounds with the heavier, less-electronegative anions, the number of broad-band electrons per cation will deviate from an integral number by, at most, only a small fraction in stoichiometric, two-component compounds. Measurements of charge-carrier mobilities would indicate whether the Fermi level falls in a partially filled, narrow band.

In the right and left columns of Table II are summarized the major assumptions of the two limiting theories: molecular-orbital theory for the broad-band case $R \ll R_c$, and ligand-field theory for the case $R > R_c$. The problem is to find a Hamiltonian that is satisfactory for the case where some d-like states are localized ($R > R_c$) and some are collective ($R < R_c$). If the smallest cation-cation separations correspond to $R = R_c - \delta R$, so that the corresponding bandwidths $\Delta\epsilon$ are small relative to the cubic component of the ligand-field splittings, then the appropriate Hamiltonian is that given by the middle column, or

$$H = H_o + V_{el} + V_{cf} + V_{LS} + H_{ep} + H_L + H_1 + H_{corr} \quad , \quad (16)$$

where $H_o + V_{el} + V_{cf} + V_{LS}$ are the single-cation energies that enter standard ligand-field theory, $H_{ep} + H_L$ represent the electron-phonon interactions and lattice energies, respectively, H_1 introduces a perturbing periodic potential that gives rise to a finite bandwidth, and H_{corr} is a collective-electron correlation energy.

The ligand-field effect consists of at least three components:

$$V_{cf} = V_o + V_c + V_{nc} \quad , \quad (17)$$

where V_o is just a constant, V_c is the cubic component, and V_{nc} is the noncubic component, which usually reflects trigonal, tetragonal, or orthorhombic symmetry. Term splittings due to V_c are anticipated to be $\Delta_c \sim 2$ ev. Intra-atomic exchange splittings due to V_{el} , the correction to the one-electron spherical approximation of H_o , are also $\Delta_{ex} \sim 2$ ev. Splittings due to V_{nc} are usually smaller than ~ 0.5 ev; they will therefore be smaller than the bandwidths to be associated with collective electrons. This is also true of the spin-orbit splittings induced by V_{LS} .

In the special case of a single charge carrier in a narrow band, the correlation terms V_{cf} and H_{corr} are not present. In this case, there is no band narrowing as a result of electron correlations, and it is tempting to apply the usual MO theory. However, even in this case the theory must be modified to account for strong electron-phonon interactions. In this special case, the one-carrier model of polaron theory is applicable. In polaron theory, $H_{ep} + H_L$ are

TABLE II
SUMMARY OF MAJOR ASSUMPTIONS IN DESCRIPTIONS OF OUTER ELECTRONS

<p>($\Delta\epsilon$ = bandwidth, τ = relaxation time between electron collisions, μ = electron mobility, $U_p(r)$ = Periodic potential due to atomic cores plus average charge distribution of all other outer electrons, H_{ep} = electron-phonon interactions, usually taken proportional to the atomic displacements, $H_a = -(\hbar^2/2m)\nabla^2 - eU(r)$, where $U(r)$ is the atomic potential due to atomic core plus average charge distribution of all other outer electrons at the atom, V_{el} = intra-atomic correlation correction for spherical approximation in H_a, V_{cf} and V_{LS} are crystal-field and spin-orbit interactions, and $H_{ex} = -\sum_{ij} J_{ij} \cdot S_i \cdot S_j$ is the Heisenberg exchange Hamiltonian.)</p>		
Molecular-Orbital Theory	Polaron Theory	Ligand-Field Theory
<p>$R \approx R_a^{nl}$ or $\Delta\epsilon \gg \hbar/\tau$ whence $\mu \gg 2 \text{ cm}^2/\text{v-sec}^\dagger$</p> <p>$H = -(\hbar^2/2m)\nabla^2 - eU_p(r) + H_{ep}$</p> <ol style="list-style-type: none"> 1. Single electron in periodic potential. Collective electron belongs to entire crystal, and Bragg scattering introduces crystal symmetry via Brillouin zones. 2. Disregard of multiplet structure at individual atoms. Although parallel-spin correlations are introduced in a Hartree-Fock solution, correlations between electrons with antiparallel spins are inadequately handled. 3. Electron-lattice interactions due to thermal vibrations or lattice defects are treated as a small perturbation. 	<p>$R \approx R_c^{nl} - \Delta R$ or $\Delta\epsilon \sim \hbar/\tau$ whence $0.5 \text{ cm}^2/\text{v-sec} < \mu < 10 \text{ cm}^2/\text{v-sec}^\dagger$</p> <p>$H = H_a + V_{el} + V_{cf} + V_{LS} + H_L + H_1 + H_{corr}$</p> <ol style="list-style-type: none"> 1. Atomic electron subject to electron-phonon interactions H_{ep} that are made collective via a perturbing periodic potential $H_1 = -e[U_p(r) - U(r)]$. $H_L = T_L + V_L$ is energy of nuclei. Crystal symmetry introduced via H_1 and a correlation perturbation H_{corr}. In the ligand-field limit, $H_1 + H_{corr} \rightarrow H_{ex}$. 2. Multielectron problem with $H = H_a + V_{el} + V_{cf}$ may be used first to separate narrow bands provided crystal-field splitting is $\Delta_{cf} > \Delta\epsilon$; multiplet structure via V_{LS} provided $\Delta_{LS} > \Delta\epsilon$. 3. Electron-lattice interactions sufficiently strong that $H_{ep} > eU_p(r)$, but $U_p(r)$ is significant enough to broaden the level into a narrow band. 	<p>$R > R_c^{nl}$ or $\Delta\epsilon \ll \hbar/\tau$ whence $\mu \ll 0.6 \text{ cm}^2/\text{v-sec}^\dagger$</p> <p>$H = H_o + V_{el} + V_{cf} + V_{LS} + V_{\lambda} + H_{ex}$</p> <ol style="list-style-type: none"> 1. Atomic (localized) electron subject to crystalline fields V_{cf}, magnetic-exchange interactions H_{ex}, and, if electron-ordering distortions occur, cooperative elastic coupling V_{λ}. Crystal symmetry introduced via $V_{cf} + V_{\lambda} + H_{ex}$. 2. Multielectron problem preserves multiplet structure via V_{LS} and intra-atomic spin correlations via V_{el}, interatomic spin correlations via H_{ex}. 3. Electron-lattice interactions so strong that localized electrons can only hop from one site to a neighboring site. In place of the periodic-potential perturbation H_1 there is a near-neighbor potential perturbation $H_1' = -e[U_{nn}(r) - U(r)]$, which enters the transfer integral b_{ij} appearing in J_{ij}^{ex} of H_{ex}.

† To estimate polaron mobilities, note that for the band model to hold $\Delta\epsilon \gg \hbar/\tau$, where $\mu = e\tau/m^*$ and $\Delta\epsilon \sim \hbar^2 k_a^2/2m^*$. Since $k_a \sim \pi/a$, where a is the lattice parameter, $\mu \gg 2 \text{ cm}^2/\text{v-sec}$ is required. For the hopping model to hold, require the lattice vibration frequency to be $\nu_L \gg W$, where the hopping probability W is related to the mobility via the Einstein diffusion expression: $\mu = Wea^2/kT$. This requirement means $\mu \ll 0.6 \text{ cm}^2/\text{v-sec}$ at 300°K.

taken to be as large or larger than the perturbing periodic potential $H_1 = -e [U_p(\vec{r}) - U(\vec{r})]$. This leads to a temperature-dependent bandwidth.

In most cases, however, there are one or more d electrons per cation present, and electron correlations tend to induce electron localization as well as the spin correlations responsible for magnetic properties. Since polaron-polaron interactions are large, it is not clear how the predictions from a one-polaron model are to be extrapolated to the many-electron case. Therefore, it is reasonable to assume that the critical separation R_c is determined primarily by the correlation energies. The electrostatic energy $U \sim \epsilon_g$ is an electron-correlation energy. However, even in the collective-electron limit $e_g \rightarrow 0$, electron correlations H_{corr} are important and may introduce splittings that are a large fraction of the bandwidth. In the limit $R > R_c$, $H_{\text{corr}} + H_1 \rightarrow H_{\text{ex}}$, where $H_1 \rightarrow H'_1$ enters the transfer integrals b_{ij} of Eq. (1). Since H_{corr} influences the relative stabilities within $\Delta\epsilon$ of the collective-electron states having different spin correlations, it determines, as a function of the position of the Fermi level E_F relative to the band, the sign of any magnetic coupling via cation-cation interactions having $R = R_c - \delta R$. As has already been indicated, it will be assumed that the sign of the magnetic couplings can be obtained from a simple extrapolation of the predictions from Eq. (1) for the case $R > R_c$. It is this assumption that leads to definite predictions about the magnetic properties of materials; therefore, a concern of this paper is to make predictions that can be checked experimentally in a meaningful way.

The many-electron correlation effects are not easily incorporated into simple one-electron energy diagrams. Both the exchange splittings for electrons of different spin and the relative stabilities of the one-electron states of a given spin depend upon the number of electrons that are present. In this report, different schematic one-electron energy diagrams are given for the cases of Pauli paramagnetism, antiferromagnetism and ferromagnetism.

B. The MnP (B31) Structure

The B31 structure of MnP may be pictured as a distortion of the hexagonal NiAs ($B8_1$) structure in which the metal atoms are displaced from the center of symmetry of the anion interstice toward one another. The orthorhombic B31 structure is illustrated in Fig. 2, where the

Fig. 2. The B31 structure of orthorhombic MnP.

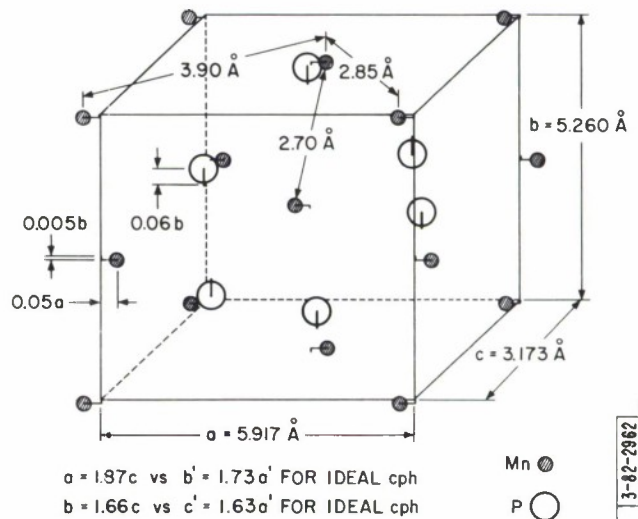


TABLE III									
ROOM TEMPERATURE CATION-CATION SEPARATIONS, IN ANGSTROMS, OCCURRING IN B31 STRUCTURES.† SEPARATION R ₁ IS ALONG [010], R ₂ AND R ₃ ARE IN (010). KNOWN ALTERNATE AB STRUCTURES ARE ALSO INDICATED, WITH SHORT METAL-METAL DISTANCES									
(Data from W.P. Pearson, "A Handbook of Lattice Spacings and Structures of Metals and Alloys," Pergamon Press (1958) and R.D. Heyding and L.D. Calvert, Can. J. Phys. 35, 449 (1957); 39, 955 (1961). The Notation B ₁ Stands for NbAs Structure as Described by H. Boller and E. Parthe, Acta Cryst. 16, 1095 (1963).)									
3d	4d	5d	R _c ^{nd‡}	P	As	Sb	Si	Ge	Sn
Ti			3.24	B ₁ (2.91)	B ₁ (3.07)	BB ₁ (3.15, 4.06)			
	Zr		4.12	B ₁ (3.13)	B ₁ (3.42)				
		Hf	4.60	B ₁ (3.32)	B ₁ (3.40)				
V			3.21	BB ₁ (3.12, 3.19)	3.04, 2.93, 3.34	BB ₁ (2.72, 4.27)			
	Nb		4.09	B ₁ (3.30, 3.34)	B ₁ (3.39, 3.45)				
		Ta	4.57	B ₁ (3.30, 3.33)	B ₁ (3.39, 3.44)				
Cr			3.18	2.76, 2.91, 3.12	2.97, 2.94, 3.49	BB ₁ (2.73, 4.13)	820	820	
	Mo		4.06	B ₁ (3.19, 3.22)					
		W	4.54	3.03, 2.73, 3.25					
Mn			3.15	2.70, 2.85, 3.17	2.85, 3.1, 3.63§	BB ₁ (2.88, 4.14)	820		
Fe			3.12	2.66, 2.78, 3.10	2.82, 2.85, 3.38	BB ₂ (2.57, 4.11)	820		835
	Ru		4.00	2.78, 2.96, 3.17	3.15, 3.2, 3.25		82		
Co			3.03	2.60, 2.76, 3.28	2.68, 2.86, 3.52¶	BB ₁ (2.60, 3.87)	820	#	835
	Rh		3.91		3.03, 3.3, 3.58	3.06, 3.12, 3.87	820	2.93, 3.07, 3.26	820
		Ir	4.39				#	2.91, 2.96, 3.49	BB ₁ (2.78, 3.99)
Ni			3.06		BB ₁ (2.53, 3.96)	BB ₁ (2.57, 3.92)	2.69, 2.69, 3.35	2.75, 2.89, 3.43	
	Pd		3.94			BB ₁ (2.80, 4.08)	2.88, 2.88, 3.38	2.98, 2.94, 3.48	2.96, 3.02, 3.87
	Pt		4.42			BB ₁ (2.74, 4.14)	2.87, 2.97, 3.60	2.95, 3.03, 3.70	BB ₁ (2.72, 4.11)
† The structure of AuGa, although B31, is significantly different from the other B31 structures, which are tabulated above.									
‡ Corresponds to metallic limit with Δ[J(J + 1)] = 0.									
§ B31 symmetry in temperature interval 45°C < T < 130°C. Elsewhere BB ₁ (2.85, 3.72).									
¶ BB ₁ symmetry above 960°C.									
# Structure not reported.									

displacements of the ions from their positions in an ideal $B8_1$ structure are indicated. The phosphor anions are displaced along the hexagonal c-axis (orthorhombic b-axis) as a result of shortening two out of six metal-metal distances in the basal planes. This suggests that the peculiar symmetry of the B31 structure is due to metal-metal bonding via d electrons. It would then illustrate but one of a large class of distortions, the low-temperature forms of VO_2 and FeS being two other examples.^{1,24} The relatively large cation displacements, corresponding to ΔR of Eq. (11), suggest that the shortest Mn-Mn separation in the a-c plane has $R < R_c^{Mn}$, the largest has $R > R_c^{Mn}$, and the intermediate has $R \approx R_c^{Mn}$.

From Eq. (15) it is estimated that

$$R_c^{Mn}(MnP) \approx (3.05 \pm 0.15) \text{ \AA} \quad , \quad (18)$$

the uncertainty being due to ignorance of the amount of increase in R_c to be anticipated on going from oxides to phosphides as a result of the greater covalence to be associated with the phosphor anion. This estimate is seen to be compatible with the inference from crystallographic symmetry that $R_{eq} - \Delta R = 2.85 \text{ \AA} < R_c^{Mn}(MnP)$ and $R_{eq} + \Delta R' = 3.90 \text{ \AA} > R_c^{Mn}(MnP)$. It also indicates that along the orthorhombic c-axis $R_{tt}^c = 3.173 \text{ \AA} > R_c^{Mn}(MnP)$, but that R_{tt}^c is sufficiently close to R_c that a temperature-dependent J_{ij}^{ex} can be anticipated for c-axis magnetic coupling.

It is concluded, therefore, that the structure of MnP is illustrative of a distortion to lower symmetry as a result of metal-metal bonding. What appears to distinguish the distortions in MnP from other members of this class that have been identified, like VO_2 and FeS , is that $T_t = T_{mp}$ rather than $T_t < T_{mp}$.

In order to check this hypothesis further, it is necessary to consider other compounds that have the B31 structure. These are listed in Table III, where the three shortest metal-metal distances are given for each case. The first thing to note is that with the exception of AuGa, whose parameters mark it as a special case, all compounds having the B31 structure have outer d shells that contain between two and six electrons. This is compatible with d-electron bonding within the two shortest distances. However, it requires that where there are six d electrons, orbitals of e_g symmetry must be partially occupied. Otherwise, the d orbitals responsible for bonding would be completely filled (see the discussion of Sec. III-C). Whether this requirement is met can be determined by measurements of χ_m , and such experiments are in progress.

The second point to note is that, with the exception of MnAs, the B31 structure is found only if the anions are sufficiently small that the two smallest cation-cation separations are smaller than R_c^{nd} . [For a generalization of Eq. (15), refer to Appendix A.] In MnAs, where the displacements are much smaller than in the other examples, $T_t < T_{mp}$. In fact, the phase only appears in the temperature interval $45^\circ\text{C} < T < 130^\circ\text{C}$. MnAs represents a special case. It will be discussed elsewhere.

If the B31 structure is caused by metal-metal bonding in the basal planes of the $B8_1$ structure, it cannot occur with only one outer d electron at the cation, since this electron is stabilized by the ligand fields into orbitals directed along the c-axis. Therefore, it is significant that the B31 structure is not found in titanium, zirconium, and hafnium phosphides, arsenides, or antimonides. From Fig. 1, homopolar bonding between cation pairs permits greater metal-metal bonding energy than bonding-band formation along a linear chain. Therefore, it is also significant that where there is one outer d electron, the B_1 structure, which contains metal-metal pairs along the c-axis at an $R < R_c$, is commonly found. The low ratio

$c/a = 1.29$ found in TiSb with $B8_1$ structure indicates bonding-band formation along the c -axis chains having $R < R_c$.

The B_t and B_h structures are characterized by metal atoms in trigonal prisms rather than octahedral sites. This geometry permits an equalization of the metal-metal bonds. Therefore, these structures are competitive with $B31$ if there is more than one outer d electron and $R < R_c$ for all near-neighbor metal-metal bonds. The fact that VP has been reported to be $B8_1$ rather than $B31$ or B_t is the only irregularity in Table III.

Finally, it is noted that compounds with Si, Ge, or Sn may have the $B20$ structure. This structure is illustrated in Fig. 3, where it is pictured as a distortion from the cubic zinc-blende structure as a result of metal-metal bonding that reduces the number of near neighbors in the

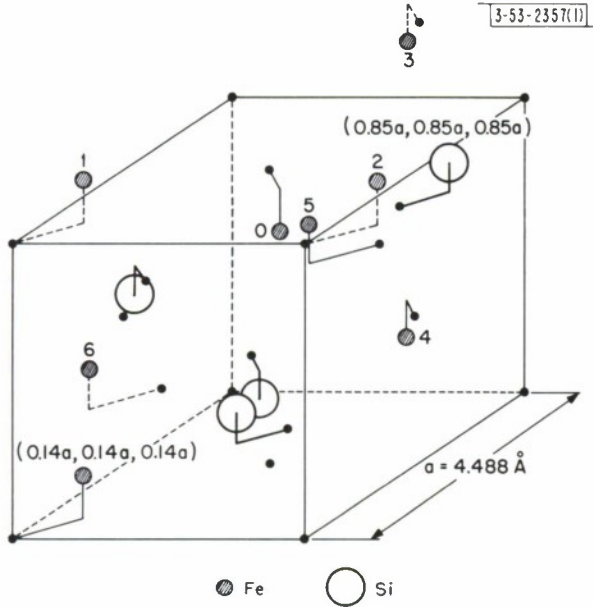


Fig. 3. The $B20$ structure of FeSi. Cation Fe_0 has six iron near neighbors at 2.76Å : Fe_1 through Fe_6 .

transition-metal sublattice from twelve to six. Thus, the $B20$ structure appears to illustrate the same class of distortion as found in the $B31$ structure, but to represent a distortion from the cubic ZnS structure rather than from the hexagonal $NiAs$ structure. The lighter Group IV elements favor the cubic ZnS structure if four transition-element electrons are stabilized relative to the d states in a bonding valence band. Therefore, it is not surprising to find the $B20$ structure competing successfully where it appears in Table III. A recent neutron-diffraction study²⁵ of FeSi is discussed from this point of view in Appendix B.

C. Construction of Energy Diagrams

1. MnP, Which Represents d^4

In order to obtain an energy level scheme from the Hamiltonian of Eq. (11), the customary procedure is to turn on successive perturbations. The nominal formula $Mn^{3+}P^{3-}$ gives correctly the number of d -like electrons per cation provided the Fermi level falls in the energy gap between valence and conduction s - p bands.

The first question to be settled is the relative magnitudes of the perturbations V_{el} and V_c , for this determines whether the ground state is a quintet or a triplet. In an octahedral ligand

field, the ${}^5\Gamma_3$ state of $\text{Mn}^{3+}(3d^4)$ has an energy $-0.6\Delta_c + 6B + 5C$, where B and C are the Racah parameters and $\Delta_c = 10Dq$ is the cubic-field splitting between states of e_g (or γ_3) symmetry and those of t_{2g} (or γ_5) symmetry.²⁶ It follows that the Mn^{3+} ion is in a low-spin (triplet) state if

$$\Delta_c > 6B + 5C \quad (19)$$

but is in a high-spin (quintet) state if the inequality is reversed. Since calculations of these parameters are not reliable, estimates of the two energies are best obtained from experiment. With the assumption $C = 4B$, it is possible to obtain values for Δ_c and B from optical spectra of the complexes. Direct experimental evidence from a MnP_6 complex is not available, but reasonable extrapolation from tabulated data²⁷ suggests $B \approx 700 \text{ cm}^{-1}$ and $\Delta_c \approx 19,000 \text{ cm}^{-1}$, which means that Δ_c and $6B + 5C \approx 26B$ have comparable energies of $\sim 2.4 \text{ eV}$, and it is not possible to predict unambiguously whether the manganese is in a high-spin or a low-spin state in MnP . It is possible to assert, however, that Δ_c decreases in progressing along the series MnP , MnAs , MnSb , MnBi . Therefore, the fact that MnAs , MnSb , and MnBi , which have the hexagonal $B8_1$ structure, all exhibit high-spin-state atomic moments of $3.4 - 4.0 \mu_B$ is not inconsistent with low-spin-state manganese in MnP . Because MnP exhibits a low ($\lesssim 2 \mu_B$) atomic moment, it is assumed that $\Delta_c > 6B + 5C$ in MnP .

The intra-atomic exchange energy is given by

$$H_{\text{ex}}^{\text{intra}} = - \sum_{m,n} J^{\text{intra}} \vec{s}_m \cdot \vec{s}_n = \begin{cases} -3J^{\text{intra}} & \text{for } {}^5\Gamma_3 \\ -\frac{3}{2}J^{\text{intra}} & \text{for } {}^3\Gamma_4 \end{cases} \quad (20)$$

where $s = 1/2$ and m, n run over the electrons at one cation. The difference in exchange stabilization between the two states would be the energy $6B + 5C$ were all the d electrons localized. With some nonlocalized electrons this may be reduced slightly, so that

$$\Delta_{\text{ex}} \approx \frac{3}{2} J^{\text{intra}} \approx 2 \text{ eV} \quad (21)$$

These splittings are indicated in Fig. 4(a).

The next perturbation to be considered is the noncubic component to the ligand field. In the hexagonal $B8_1$ structure there is a trigonal component to the ligand fields that stabilizes from the three t_{2g} orbitals a $\Gamma_{T1} \sim (2z'^2 - x'^2 - y'^2)/r^2$, where z' is along the c -axis, relative to two degenerate Γ_{T3}^1 and Γ_{T3}^2 orbitals. The distortion to the orthorhombic symmetry of $B31$ splits these two degenerate orbitals as well as the twofold-degenerate e_g orbitals. Splittings by the orthogonal fields are shown in Fig. 4(b). So long as the relative positions of the $E_{01}(\uparrow)$ and $\Gamma_{03}^1(\downarrow)$ levels are maintained, the absolute magnitudes of the splittings Δ_0 and δ_0 are not important for the magnetic properties of MnP .

It has already been pointed out that, according to Eq. (18) and Fig. 2, $R < R_c^{\text{Mn}}(\text{MnP})$ for the orbitals Γ_{01} and Γ_{03}^1 , that $R \gtrsim R_c^{\text{Mn}}(\text{MnP})$ for the Γ_{03}^2 orbital. Therefore, the Γ_{01} and Γ_{03}^1 levels must be broadened into narrow ($\sim 1.0 \text{ eV}$) bands. These bands undoubtedly overlap to give one band of width $\Delta\epsilon < \Delta_{\text{ex}}$. The Γ_{03}^2 states, on the other hand, form narrow bands of localized states. The e_g states, which are directed toward the anions, are even more sharply localized. A schematic density-of-states curve is shown in Fig. 4(c). In MnP , the bandwidth $\Delta\epsilon$ is not

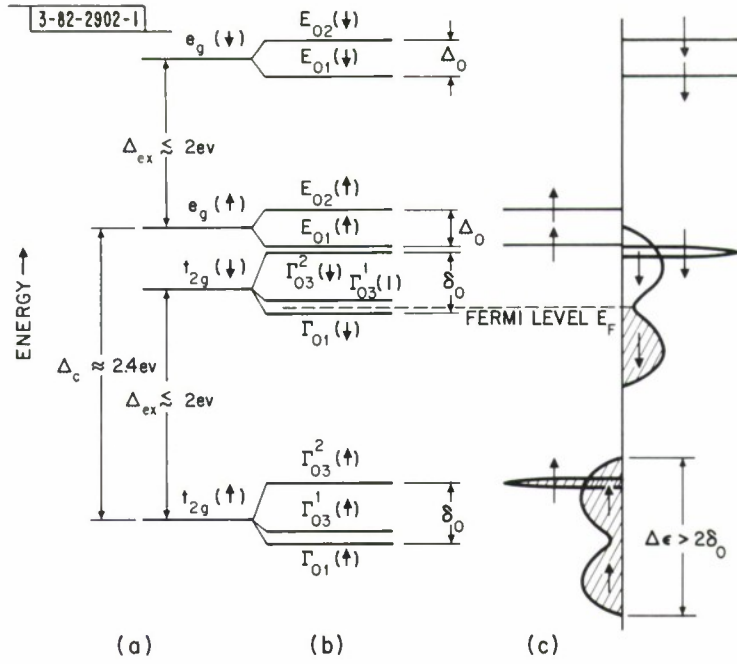


Fig. 4. Schematic one-electron diagram for d-like states of MnP. (a) Cubic-field splittings; (b) total ligand-field splittings; (c) energy-band diagram for collective-electron ($\Gamma_{01} + \Gamma_{03}^1$) states having a bandwidth $\Delta\epsilon$, where $\delta_0 < \Delta < \Delta_{ex}$. The energies δ_0 and Δ_{ex} represent orthagonal-field and intra-atomic-exchange splittings, respectively.

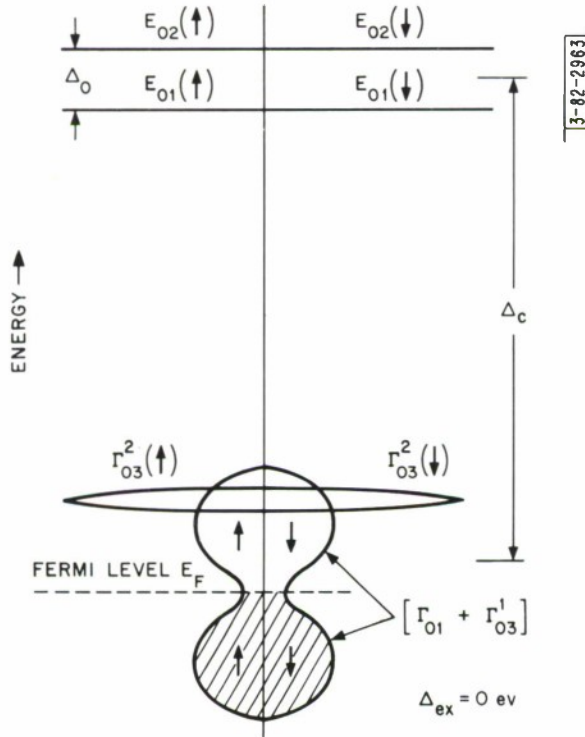


Fig. 5. Schematic one-electron energy diagram for d-like states of VAs. $\Delta_{ex} = 0$ and filled $\Gamma_{01} + \Gamma_{03}^1$ states are bonding; empty $\Gamma_{01} + \Gamma_{03}^1$ states are antibonding.

important for predictions about the magnitude of the atomic moment and the signs of the various magnetic couplings; neither is the shape of the density-of-states curve within a band. Intra-atomic correlations from V_{el} shift the states corresponding to one spin relative to those corresponding to the opposite spin by Δ_{ex} . Interatomic correlations from H_{corr} stabilize bonding states, destabilize antibonding states. This effect is represented by the bimodal character of the bands of a given spin.

2. VAs, Which Represents d^2

In the case of VAs, there are only two d-like electrons per molecule, and these occupy the Γ_{01} and Γ_{03}^1 orbitals, which are broadened into narrow bands of collective-electron states. Since there are no localized electrons present, there is no localized atomic moment to induce a local molecular field, and hence to trigger an exchange splitting Δ_{ex} . This modifies the density-of-states curves from those of Fig. 4 to those of Fig. 5.

3. CrAs, Which Represents d^3

CrAs contains three d-like electrons per molecule, and the magnetic properties depend upon whether $\Delta\epsilon$ is large enough that the Fermi level overlaps the localized Γ_{03}^2 states. If it does, there is a molecular field present to induce an exchange splitting $\Delta'_{ex} < J^{intra}$. (The inequality sign indicates the reduction in J^{intra} caused by the presence of some collective electrons. This reduction will be greater for antiferromagnetic than for ferromagnetic compounds.) This leads to the energy diagram of Fig. 6. Since there are two collective electrons and two collective orbitals per cation, it is predicted from extrapolation of Eq. (1) that CrAs is antiferromagnetic. Therefore, it is helpful to show the density-of-states curves for two magnetic sublattices. Note that if $\Delta'_{ex} > \Delta\epsilon$, as shown in Fig. 6, there is an energy gap between a filled and an empty band. This means that stoichiometric, antiferromagnetic CrAs could be a semiconductor.

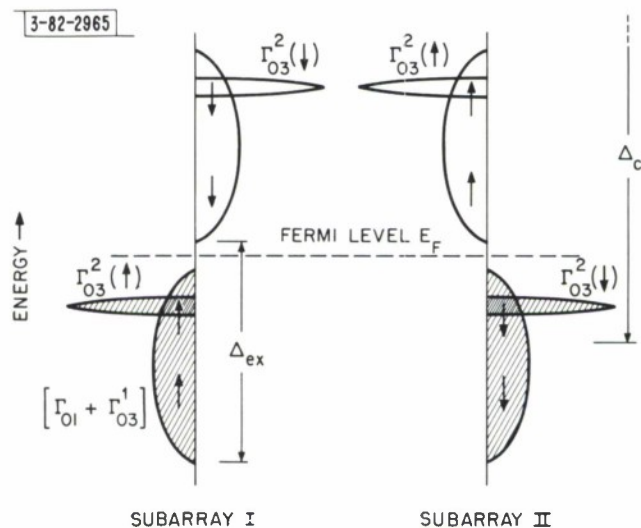


Fig. 6. Schematic one-electron energy diagram for Γ_{01} and $\Gamma_{03}^{1,2}$ states of the chromium sublattice in antiferromagnetic CrAs. Occupied states are banding states.

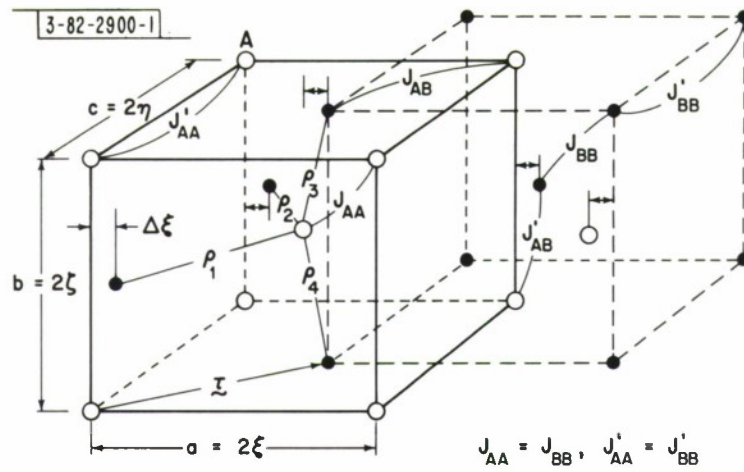


Fig. 7. Two-subarray model for cation sublattice of orthorhombic B31 structure. Definitions of exchange parameters and coordinates.

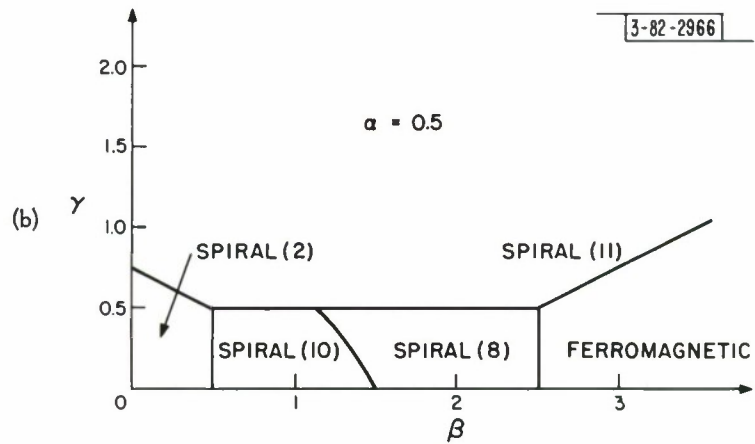
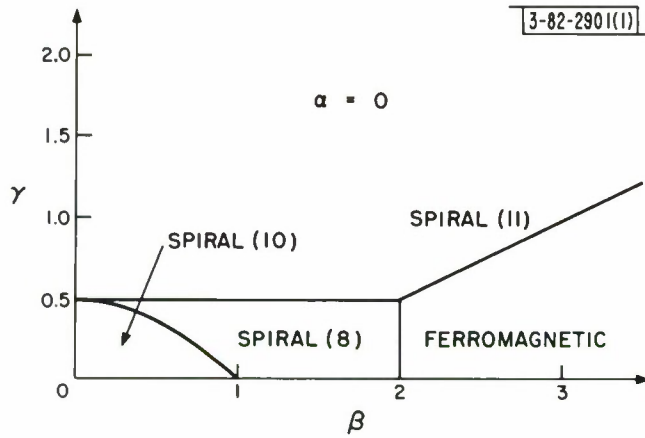


Fig. 8. Regions of stability in exchange-parameter space for various spin configurations in orthorhombic MnP.

$$\alpha \equiv (J'_{AB} - J_{AB})/J_{AB}, \beta \equiv J'_{AB}/4J_{AA}, \gamma \equiv (1 + \alpha) J'_{AA}/2J_{AA}.$$

4. FeP and CoP, Which Represent d^5 and d^6

These compounds contain, respectively, five and six outer electrons. This raises the Fermi level from its position in Fig. 4, and it is immediately apparent that the magnitude of any localized atomic moment depends critically upon the relative positions of $E_{01}(\uparrow)$ and $\Gamma_{03}^2(\downarrow)$ and on the degree they are overlapped by the band of collective states. However, it can be stated unequivocally that if the B31 structure is stabilized by metal-metal bonding, then the band of collective states must overlap both the $E_{01}(\uparrow)$ and the $\Gamma_{03}^2(\downarrow)$ states. Otherwise, the narrow-band states would be full, and they could not give rise to bonding.

D. Magnetic Order and Atomic Moment

1. MnP

It follows unambiguously from Fig. 4 that MnP can have a maximum spin-only contribution to the atomic moment of $2\mu_B$. The orbital contribution is from the antibonding electrons, which have spins parallel to the net moment and tend to be localized. This reduces the moment by a fractional Bohr magneton $f'\mu_B$. Therefore, it is predicted that

$$\mu_{Mn} = (2 - f')\mu_B \quad . \quad (22)$$

The magnetic order may be quite complicated. This problem is most easily treated by representing the cation sublattice as two interpenetrating, body-centered-orthorhombic arrays A and B, as shown in Fig. 7. Four magnetic interactions are important. These are represented by the four J_{ij}^{cx} for these interactions: J'_{AB} for nearest-neighbor interactions along the orthorhombic b axis, J_{AB} for nearest-neighbor interactions within the a-c plane, $-J'_{AA}$ for A-A or B-B interactions along the c-axis, and $-J_{AA}$ for interactions between corner and body-center cations of subarray A or B. The first two interactions are via Γ_{01} and Γ_{03}^1 electrons. Since the Γ_{01} and Γ_{03}^1 orbitals contain three electrons per orbital, extrapolation of Eq. (1) calls for ferromagnetic exchange, or positive J_{AB} and J'_{AB} . The Γ_{03}^2 orbitals, on the other hand, contain only one electron, and the c-axis interactions are antiferromagnetic. [Since $R > R_c$, Eq. (1) applies.] Therefore, $J'_{AA} = J'_{AA}(T)$ is positive and is expected to increase measurably with decreasing temperature because $R = R_c = \delta R$ and δR is small. The interactions between corner and body-center positions of a body-centered array are cation-anion-cation interactions. These interactions are most probably antiferromagnetic and are therefore represented by $-J_{AA}$, where J_{AA} is positive. This interaction is relatively weak, because the e_g orbitals are empty. Also, it is assumed that $J'_{AA} \lesssim J_{AB} < J'_{AB}$ because the cation-cation separations increase in this order, the AA interactions corresponding to $R > R_c$ and the AB interactions to $R < R_c$. (See Sec. II-B-2.)

It is convenient to define these exchange parameters via three parametric ratios:

$$\alpha \equiv \frac{J'_{AB}}{J_{AB}} - 1 \quad , \quad \beta \equiv \frac{J'_{AB}}{4J_{AA}} \quad , \quad \gamma \equiv \frac{J'_{AB}J'_{AA}(T)}{2J_{AB}J_{AA}} \quad . \quad (23)$$

In Appendix C, the ground-state spin configurations are derived from the Heisenberg exchange Hamiltonian H_{ex} , and the results in the β - γ plane for $\alpha = 0$ and $\alpha = 1/2$ are shown graphically in Fig. 8. Although $\beta > 2$ is probable, it is immediately obvious that MnP may have a complex spin configuration. However, if a complex spin configuration is stable in zero field, a

ferromagnetic phase may be induced by an external field, since a field would enlarge the ferromagnetic domain. Therefore, either ferromagnetism or metamagnetism is compatible with the qualitative predictions for the signs and relative magnitudes of the exchange parameters. It was also predicted that γ increases measurably with decreasing temperature. Therefore, if an antiferromagnetic \rightleftharpoons ferromagnetic transition is observed as the temperature is varied in zero applied field, the low-temperature phase is predicted unambiguously to be represented by spiral (11). Such an antiferromagnetic \rightleftharpoons ferromagnetic transition has been observed at 50°K.⁵

Note that spiral (11) of Fig. 8 propagates along the orthorhombic c-axis. It is pointed out in Appendix C that dipole-dipole interactions tend to stabilize the plane of the spiral perpendicular to the propagation direction. This energy of stabilization is $K_d \sim 10^6$ ergs/cm³. However, MnP has an exceptionally hard a-axis ($K_1 \approx 1.4 \times 10^7$ ergs/cm³),⁵ so that the spins of spiral (11) are forced into the b-c plane. The form of this spiral, without anisotropy within the b-c plane, is that shown in Fig. 9. This antiferromagnetic configuration requires that the initial susceptibility $\chi_m(\vec{H} \parallel \vec{a}) = \chi_a$ remain nearly constant on passing through the antiferromagnetic \rightleftharpoons ferromagnetic transition. However, χ_b and χ_c must decrease abruptly on lowering the temperature through the transition temperature.

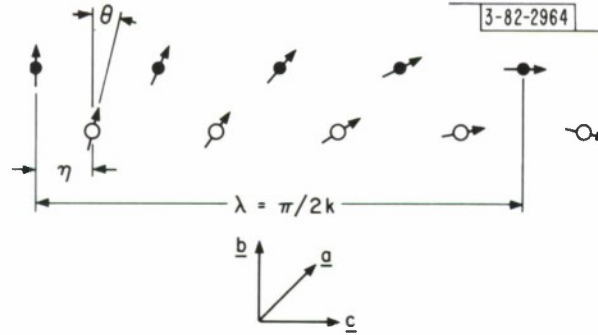


Fig. 9. Projection (with displacements of A and B sublattices exaggerated) of spiral (11) on the orthorhombic c-axis of MnP. Each arrow represents a ferromagnetic o-b plane. This spiral is modified by crystalline anisotropy and applied magnetic fields.

Although these general features have been observed, a measured $\chi_c - \chi_b \approx 2.5 \times 10^{-3}$ emu/cm³-oe shows that the simple spiral must be strongly perturbed. There are two factors that can perturb the spiral: the large anisotropy forces in the b-c plane, and exchange striction. For a uniform spiral, the turn angle between next-near-neighbor (001) planes is constant, and exchange striction will not distort the spiral even though it strongly influences the wavelength of the spiral. However, if anisotropy within the b-c plane perturbs the spiral, exchange striction can amplify the perturbation by inducing a shorter separation between next-near-neighbor (001) planes of spins that support a larger turn angle, thus locally stabilizing the J'_{AA} interaction. Since the observed antiferromagnetic \rightleftharpoons ferromagnetic transition indicates that J'_{AA} is sensitive to interatomic separation (an observation that is compatible with $2\eta \approx R_c^{Mn}$), it is clear that exchange striction must be introduced into the problem. This is done in Eq. (C-33) of Appendix C by multiplying the exchange interaction J'_{AA} by the factor $(1 - \alpha\epsilon_n)$, where ϵ_n is a local strain at the n^{th} site that is defined by Eq. (C-34) as

$$\epsilon_n = \epsilon_o \cos(\varphi_{n+2} - \varphi_n) \quad , \quad \text{and} \quad \epsilon_o = \alpha_s J'_{AA} M_s^2 / 2Y \quad .$$

Here φ_n is the angle the moment of the n^{th} (001) plane makes with the direction of an applied field \vec{H} , and Y is Young's modulus. Whereas the unperturbed spiral with turn angle Θ is described by $\varphi_n^0 = n\Theta$, the perturbed spiral is described by Eq. (C-41):

$$\varphi_n = n\Theta - \epsilon h_A \sin(2n\Theta) - h \sin(n\Theta) \quad ,$$

where $\epsilon = +1$ if $\vec{H} \parallel \vec{c}$ and $\epsilon = -1$ if $\vec{H} \parallel \vec{b}$. This leads to the perturbed spiral shown in Fig. 10 and to the observed $(\chi_c - \chi_b)$ if $\alpha \approx 15$ and $\epsilon_o \approx 0.015$ for a $\Theta = 20^\circ$. This predicts an observable modulation below 50°K of the c-axis spacing, a modulation that has a wavelength half as large as that of an antiferromagnetic spiral propagating along the c-axis.

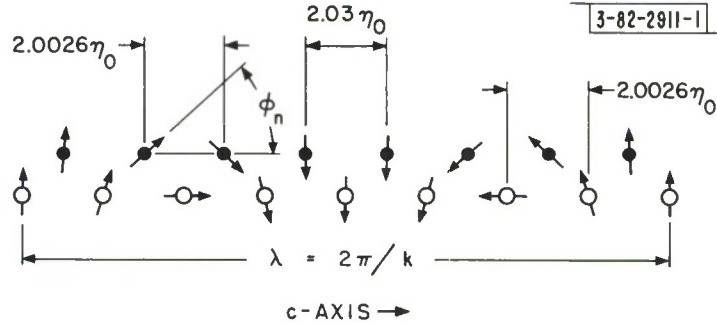


Fig. 10. Proposed spin configuration [distorted spiral (11)] for the antiferromagnetic phase of MnP given $\theta = \pi/8$, $\epsilon_o = 0.015$. The turn angle is $\phi_n = n\theta - h_A \sin(2n\theta)$, where $h_A = -2(\chi_c - \chi_b)/(\chi_c + \chi_b) = -0.5$. This gives $\phi_n = 0, \pm 42.5^\circ, \pm 73.6^\circ, \pm 106.4^\circ, \pm 137.5^\circ, \pm 180^\circ$. Both θ and ϵ_o are temperature dependent.

The critical field strength H_k for an antiferromagnetic \rightleftharpoons ferromagnetic transition below 50°K is given by Eq. (C-42). Since J'_{AA} increases with decreasing temperature via the thermal expansion coefficient, H_k must increase with decreasing temperature as found experimentally. Comparison of $H_k(T)$ with the temperature dependence of the c-axis parameter would give an independent check on the parameter α_s .

Finally, note that the temperature dependence of J'_{AA} will change the experimental paramagnetic Curie constant from C to $C_{\text{expt}} = C/(1 - CW_1)$ if the total ferromagnetic internal field can be represented by $H + (W_o + W_1 T) M$. Since J'_{AA} is an antiferromagnetic contribution that decreases with increasing temperature, $W_1 > 0$ and the spontaneous moment μ_{eff} obtained from C_{expt} may be too large.

2. VAs

It is clear from Fig. 5 that VAs has no localized d electrons. Therefore, it is predicted to have no atomic moment at 0°K . Further, if the Fermi level is at a minimum in the density-of-states curve, as indicated, $d\chi_m/dT > 0$ initially. However, χ_m must go through a maximum and approach a Curie-Weiss law at high temperatures. The asymptotic paramagnetic Curie temperature will be negative, reflecting occupied bonding states; and the molecular Curie constant should be $C \approx 3/8$, the decrease from one reflecting spin-pairing in the bonding states.

3. CrAs

For a bandwidth $\Delta\epsilon_P$ greater than the splitting of the t_{2g} levels by the noncubic components of the ligand fields, localized Γ_{03}^2 states are occupied, and there is an internal magnetic field to induce a spontaneous atomic moment. Whereas the band states contain three electrons per Γ_{01} and Γ_{03}^1 orbital in MnP, they contain only two electrons in CrAs. Therefore, extrapolation of Eq. (1) calls for antiferromagnetic AB interactions in CrAs, ferromagnetic AB interactions in MnP. With strong antiferromagnetic coupling, the band electrons tend to be spin-paired, and the internal fields can only induce a localized spin density corresponding to a fraction $f \approx 0.5$ per band electron. Therefore, from Fig. 6 it is predicted that CrAs is antiferromagnetic and has an atomic moment

$$\mu_{Cr} = (1 + 2f) \mu_B \approx 2 \mu_B \quad . \quad (24)$$

It should also be noted that the AA interactions are antiferromagnetic and competitive, just as in the case of MnP, so that the antiferromagnetic spin configuration may not be collinear. However, there is no ferromagnetic domain in exchange-parameter space in this case. Therefore, it is predicted that CrAs is not metamagnetic.

4. FeP

The band structure of FeP should be similar to that of MnP shown in Fig. 4. Its magnetic properties depend critically upon the relative stabilities of the $E_{01}(\uparrow)$ and $\Gamma_{03}^2(\downarrow)$ levels. If the $E_{01}(\uparrow)$ is the more stable, then the atomic moment is

$$\mu_{Fe} \approx (1 + 2n_h) \mu_B \sim 2 \mu_B \quad , \quad (25)$$

where n_h is the number of holes per iron atom in the band states. This moment is considerably larger than the experimental moment $\mu_{Fe} = 0.36 \mu_B$.²⁸ Although there was an apparent lack of saturation, even at 25,000 gauss, for the powder specimens investigated, the observed moment indicates that the $\Gamma_{03}^2(\downarrow)$ level is the more stable. Because the $\Gamma_{03}^2(\downarrow)$ states are not completely filled, there is a sufficient density of states at the Fermi surface for spontaneous magnetization to occur. The spin-only contribution to the atomic moment is then $1 \mu_B$, and

$$\mu_{Fe} = (1 - f') \mu_B \quad . \quad (26)$$

Not only the AB but also the c-axis AA interactions (J'_{AA}) are ferromagnetic. This increases considerably the ferromagnetic domain in interaction-parameter space, and ferromagnetism can be predicted with confidence.

IV. CONCLUSIONS

Compounds with the B31 and B20 structure appear to be representative of a large class of compounds in which distortions from a close-packed anion sublattice to lower symmetry are induced by metal-metal bonding via outer d electrons.

It is meaningful to introduce a critical metal-metal separation R_c such that for $R < R_c$ the overlapping d orbitals of neighboring cations must be described by collective, crystalline states, whereas for $R > R_c$ they may be described by localized states.

Distortions due to metal-metal bonding are most probable if $R \approx R_c$ in the undistorted configuration.

If localized and collective d electrons are simultaneously present, it is possible to obtain a qualitative energy diagram by first constructing the ligand-field diagram for localized states and then superimposing a collective-electron character on those states whose symmetry indicates overlap with near neighbors at an $R < R_c$. Because the parameters of ligand-field theory cannot now be adequately calculated from first principles, details of the energy-band scheme depend upon empirical information.

Sharp predictions of Pauli paramagnetism, antiferromagnetism, metamagnetism, and ferromagnetism as a function of d-electron/cation ratio have been made for the B31 compounds, and these predictions are in agreement with experiment where data are available. Therefore, magnetic coupling via narrow-band ($R < R_c$) states appears to have the same sign as would be predicted from superexchange theory were the states localized ($R > R_c$).

The proposed energy scheme permits interpretation of the spin-only contribution to the atomic moment and the sign of the orbital contribution.

ACKNOWLEDGMENT

I would like to thank Dr. T. A. Kaplan for several helpful discussions about Appendix C.

APPENDIX A

In order to simultaneously obtain an independent estimate of the critical separation R_c of Eq. (15) and to extend it to the 4d and 5d compounds, it is assumed that the ratio of the equilibrium separation for bonding via overlapping cationic states equals the ratio of the mean radii of the overlapping wave functions. To make use of this assumption, it is necessary to have a suitable description of the overlapping cationic states. In a solid, these are modified by covalence effects, which admix anion states and therefore increase the mean radial extension. Since the cationic states of interest are directed toward other cations and away from anions, these covalency effects are probably small, except for a special case: Cations with abnormally large charge in crystals where π bonding and σ bonding do not compete for the same anion orbitals may have larger cation-directed orbitals because of abnormally strong π bonding. This situation is found, for example, in rutile and ReO_3 structure. For other cases, it should be possible to use screened, hydrogenic wave functions. However, this introduces a factor that favors larger R_1 in Eq. (13) for crystals with greater covalency.

The assumption, then, leads to the relation

$$R_o^{n'l'}/R_o^{nl} \approx \langle r_{n'l'} \rangle / \langle r_{nl} \rangle \quad , \quad (\text{A-1})$$

where the mean atomic radius of an electron with quantum numbers n, l is given by

$$\langle r_{nl} \rangle = \int r_{nl} |\Psi|^2 d\tau = \left(\frac{na_o}{2Z_{\text{eff}}^{nl}} \right) \frac{I_{1,n+l}^l}{I_{0,n+l}^l} \quad , \quad (\text{A-2})$$

$$I_{k,n+l}^l = \int_0^\infty \rho^{2l+k} \exp[-\rho] [L_{n+l}^{2l+1}(\rho)]^2 d\rho \quad . \quad (\text{A-3})$$

The integrals in Eq. (A-3) are solved by standard procedures with the aid of the generating function for the Laguerre polynomials, and

$$\langle r_{nl} \rangle = r_n(\text{Bohr}) [(3n-l)(3n-l+1)/4n^2] \quad , \quad (\text{A-4})$$

where

$$r_n(\text{Bohr}) = n^2 (a_o / Z_{\text{eff}}^{nl}) \quad , \quad a_o = \hbar / m_e^2 = 0.53 \text{ \AA} \quad . \quad (\text{A-5})$$

Further, the atomic eigenvalues are

$$E_{nl} = - (2\mu_r e^4 / \hbar^2) (Z_{\text{eff}}^{nl} / n)^2 \quad (\text{A-6})$$

so that substitution of Eqs. (A-4), (A-5), and (A-6) into (A-1) gives

$$R \approx R_o^{nl} \left(\frac{E_{nl}}{E_{n'l'}} \right)^{\frac{1}{2}} \left(\frac{n}{n'} \right) \frac{3n'(3n'+1)}{(3n-l)(3n-l+1)} \quad , \quad (\text{A-7})$$

where R is the crystalline interatomic separation, which is taken to be the equilibrium separation for the broad-band electrons with quantum numbers $n', l' = 0$. Since partially filled d or f shells occur only where $E_{nl} \approx E_{n'l'}$, it follows that, for the rare-earth and actinide elements or the transition elements,

$$(E_{nl}/E_{n'0})^{\frac{1}{2}} \approx 1 \quad . \quad (A-8)$$

A correction must be estimated for the tendency of the d and f shells to become more tightly bound (higher $Z_{\text{eff}}^{n,\ell}$) as the atomic number increases across any row of the Periodic Table. Since it has the form

$$\Delta R = -a(Z - Z_{Ti}) \quad , \quad a > 0 \quad , \quad (A-9)$$

it is included in the estimate for R_2 in Eq. (13).

To obtain numerical estimates for R_c^{nl} , it is noted that 4f electrons are localized, whereas the 4d electrons of metallic palladium give rise to Pauli paramagnetism, characteristic of collective electrons. This means that from Eqs. (A-7) and (A-8) and the definition of R_c ,

$$R_{nn}(\text{rare-earth}) \approx 2.53 R_o^{4f} > R_c^{4f} \quad ,$$

$$R_{nnn}(\text{Pd}) \approx \sqrt{2} R_{nn}(\text{Pd}) \approx 2.47 R_o^{4d} < R_c^{4d} \quad .$$

This leads to the conclusion that for metals, R_1 of Eq. (13) is

$$R_1^{nd} \approx 2.5 R_o^{nd} \quad , \quad (A-10)$$

where, from Eq. (A-7),

$$R_o^{nd} \approx R_{nn} \frac{(3n-2)(3n-1)}{3n(3n+4)} \quad . \quad (A-11)$$

From a knowledge of the lattice parameters of Ni, Pd and Pt, it follows that for metals at room temperature,

$$\begin{aligned} R_c^{3d} &\approx 3.06 \text{ \AA} - R_2^{3d}(Z - Z_{Ti} - 6) - R_3^{3d} \Delta[J(J+1)] \quad , \\ R_c^{4d} &\approx 3.94 \text{ \AA} - R_2^{4d}(Z - Z_{Zr} - 6) - R_3^{4d} \Delta[J(J+1)] \quad , \\ R_c^{5d} &\approx 4.42 \text{ \AA} - R_2^{5d}(Z - Z_{Hf} - 6) - R_3^{5d} \Delta[J(J+1)] \quad . \end{aligned} \quad (A-12)$$

From a knowledge of ionic radii,⁽¹²⁾ it is estimated that

$$R_2^{3d} \approx R_2^{4d} \approx R_2^{5d} \approx 0.03 \text{ \AA} \quad . \quad (A-13)$$

This implies that

$$\begin{aligned} R_c^{4d} &\approx R_c^{3d} + 0.88 \text{ \AA} \quad , \\ R_c^{5d} &\approx R_c^{3d} + 1.36 \text{ \AA} \quad . \end{aligned} \quad (A-14)$$

Also note that comparison of Eq. (15) with (A-12) shows

$$R_c(\text{metals}) \approx R_c(\text{oxides}) + 0.2 \text{ \AA} \quad ,$$

which is a reassuring check on the adequacy of Eq. (A-14).

APPENDIX B

The compound FeSi has the B20 structure of Fig. 3, and each iron atom has six near-neighbor irons at $2.75 \text{ \AA} < R_c(\text{Fe})$. The symmetry about a given iron atom is trigonal, and the d-like orbital directed along the trigonal axis is rendered relatively unstable by a silicon nearest neighbor at 2.29 \AA . Given a Fermi level located between two broad bands, each iron has four d-like electrons. Since the trigonal-axis orbital is relatively unstable, these occupy collective-electron states. The cation sublattice consists of two arrays such that an atom of one array has only near neighbors belonging to the other array. Four overlapping orbitals per iron atom make the band of collective-electron states, so that at absolute zero bonding states are occupied, anti-bonding states empty, and the Fermi level is at a minimum in the density-of-states curve. Kriessman and Callen⁽²⁹⁾ have shown that $d\chi_m/dT > 0$ for collective electrons in such a case. However, χ_m cannot increase indefinitely with T; in fact, χ_m should approach a Curie-Weiss law at high temperatures. The Curie constant obtained from the asymptote to the high-temperature Curie-Weiss curve will correspond to an atomic spin density of $\sim \frac{1}{4}$ per collective electron, the effective spin magnitude being reduced by spin-pairing within the bonding states. Also, the paramagnetic Curie temperature would be negative, reflecting the antiparallel correlations within the bonding states. Finally, there would be no localized atomic moment at 0°K , since all the occupied states are collective. The situation should be analogous to that predicted for VAs.

Benoit⁽³⁰⁾ and others⁽²⁵⁾ have measured the magnetic susceptibility of FeSi as a function of temperature. Although the results are sensitive to sample preparation, so that the details of the two investigations are different, each found a broad maximum in χ_m vs T near 200°C , a negative paramagnetic Curie temperature, and a molar Curie constant between 0.64 and 0.83. Although this might be interpreted to indicate antiferromagnetism, Watanabe, Yamamoto and Ito⁽²⁵⁾ found no coherent antiferromagnetic intensity in neutron diffraction either at room temperature or at liquid-nitrogen temperature. Therefore, localized atomic moments are apparently not present, at least at low temperature.

If cation-cation bonding is responsible for the B20 structure, no additional bond formation can occur below 200°C , so that the situation is to be contrasted with the susceptibility changes occurring at the first-order phase transitions of VO_2 or V_2O_3 .⁽¹⁾ The neutron data did not indicate any pronounced cation shifting in FeSi on passing through 200°C .

APPENDIX C

To obtain the ground-state spin configuration for MnP as a function of the relative strengths of the various competitive exchange interactions, use is made of the Lyons-Kaplan³ formalism for this type of problem. If only exchange energy is important, the Hamiltonian is

$$H_{\text{ex}} = - \sum_{n\nu, m\mu} J_{n\nu, m\mu} \vec{S}_{n\nu} \cdot \vec{S}_{m\mu} \quad , \quad (\text{C-1})$$

which is subject to the strong constraint

$$\vec{S}_{n\nu} \cdot \vec{S}_{n\nu} = S_\nu^2 \quad . \quad (\text{C-2})$$

By the Luttinger-Tisza³¹ theorem, if the solution to the weak constraint problem also satisfies the strong constraints, then the weak-constraint solution is the solution for the strong-constraint problem. The weak constraint is

$$\sum_{n, \nu} \vec{S}_{n\nu} \cdot \vec{S}_{n\nu} = NS^2 \quad ,$$

where N is the number of manganese atoms. With the two-subarray model of Fig. 7 for the cation sublattice, the subscript ν refers to the two subarrays A and B, and a lattice vector is defined as

$$\vec{R}_{n\nu} = \vec{R}_n + \vec{\rho}_\nu \quad . \quad (\text{C-3})$$

Since the exchange interactions are reciprocal,

$$J_{n\nu, m\mu} = J_{\nu\mu}(\vec{R}_m - \vec{R}_n) = J_{\mu\nu}(\vec{R}_n - \vec{R}_m) \quad . \quad (\text{C-4})$$

The Fourier transforms for the spin vectors are

$$\vec{S}_{n\nu} = \sum_{\vec{k}} \exp[i\vec{k} \cdot \vec{R}_{n\nu}] \vec{Q}_{\vec{k}\nu} \quad , \quad \vec{S}_{m\mu} = \sum_{\vec{k}} \exp[i\vec{k} \cdot \vec{R}_{m\mu}] \vec{Q}_{\vec{k}\mu} \quad , \quad (\text{C-5})$$

and Eq. (C-1) yields an energy density

$$\epsilon = E/N = 2 \sum_{\vec{k}} \sum_{\nu\mu} L_{\nu\mu}(\vec{k}) \vec{Q}_{\vec{k}\nu}^* \cdot \vec{Q}_{\vec{k}\mu} \quad ,$$

where

$$L_{\nu\mu}(\vec{k}) = - \sum_{\vec{R}_m - \vec{R}_n} \exp[i\vec{k} \cdot (\vec{R}_{m\mu} - \vec{R}_{n\nu})] J_{\nu\mu}(\vec{R}_m - \vec{R}_n) = L_{\mu\nu}^*(\vec{k}) \quad . \quad (\text{C-6})$$

The weak constraint becomes

$$\sum_{\vec{k}} \sum_{\nu} \vec{Q}_{\vec{k}\nu}^* \cdot \vec{Q}_{\vec{k}\nu} = 2S^2 \quad , \quad (\text{C-7})$$

and by the method of Lagrange multipliers,

$$2 \sum_{\mu} L_{\nu\mu}(\vec{k}) \vec{Q}_{\vec{k}\mu}^* = -\lambda \vec{Q}_{\vec{k}\nu} \quad , \quad (\text{C-8})$$

so that

$$\epsilon = -\lambda \sum_{\vec{k}} \sum_{\nu} \vec{Q}_{\vec{k}\nu}^* \cdot \vec{Q}_{\vec{k}\nu} = -2\lambda S^2 \quad . \quad (\text{C-9})$$

Therefore, the ground-state configuration is that which maximizes λ , where λ is defined by Eq. (C-8). Given the two subarrays A and B, Eq. (C-8) gives

$$\begin{pmatrix} L_{AA} & L_{AB} \\ L_{AB}^* & L_{BB} \end{pmatrix} \begin{pmatrix} \varphi_1 \\ \varphi_2 \end{pmatrix} = -\frac{\lambda}{2} \begin{pmatrix} \varphi_1 \\ \varphi_2 \end{pmatrix} \quad , \quad (\text{C-10})$$

where use has been made of the relation: $L_{\nu\mu}(\vec{k}) = L_{BA} = L_{\mu\nu}(\vec{k}) = L_{AB}^*$. Further, since $\vec{R}_{mA} + \vec{\tau} = \vec{R}_{mB}$, it follows immediately from (C-6) that

$$L_{AA} = L_{BB} = -a \quad .$$

Also, $L_{AB} = -\beta \exp[i\gamma]$, where β is real and positive, so that Eq. (C-10) has the eigenfunctions $\varphi_1 = 1$, $\varphi_2 = \exp[i\varphi]$ with the eigenvalues

$$\frac{\lambda}{2} = \begin{cases} (a + \beta) & \text{if } \varphi = -\gamma \\ (a - \beta) & \text{if } \varphi = \pi - \gamma \end{cases} \quad .$$

From Eq. (C-8), this means that $\vec{Q}_{\vec{k}B} = \vec{Q}_{\vec{k}A} \exp[i\varphi]$. Choose

$$\vec{Q}_{\vec{k}A} = \frac{1}{2} \hat{x} + \frac{1}{2i} \hat{y} \quad , \quad (\text{C-11})$$

and Eq. (C-5) gives

$$\vec{S}_{\vec{k}n_A} = \hat{x} \cos \vec{k} \cdot \vec{R}_{n_A} + \hat{y} \sin \vec{k} \cdot \vec{R}_{n_A} \quad , \quad (\text{C-12})$$

$$\vec{S}_{\vec{k}n_B} = \hat{x} \cos(\vec{k} \cdot \vec{R}_{n_B} + \varphi) + \hat{y} \sin(\vec{k} \cdot \vec{R}_{n_B} + \varphi) \quad ,$$

and

$$\vec{S}_{\vec{k}n_A} \cdot \vec{S}_{\vec{k}n_A} = \vec{S}_{\vec{k}n_B} \cdot \vec{S}_{\vec{k}n_B} = 1 \quad . \quad (\text{C-13})$$

This shows that the solution to the weak-constraint problem satisfies the strong-constraint problem; and the many-body problem reduces to maximizing λ with respect to \vec{k} , the wave vector for a flat spiral, where

$$\frac{\lambda}{2} = -L_{AA} + |L_{AB}| \quad . \quad (\text{C-14})$$

From Fig. 7, it follows that

$$\begin{aligned} -L_{AB} &= J_{AB} \{ \exp [i\vec{k} \cdot \vec{\rho}_1] + \exp [i\vec{k} \cdot \vec{\rho}_2] \} + J'_{AB} \{ \exp [i\vec{k} \cdot \vec{\rho}_3] + \exp [i\vec{k} \cdot \vec{\rho}_4] \} \\ &= 2J_{AB} \exp [i\vec{k} \cdot (-\vec{\xi} + \Delta\vec{\xi})] \cos \vec{k} \cdot \vec{\eta} + 2J'_{AB} \exp [i\vec{k} \cdot \Delta\vec{\xi}] \cos \vec{k} \cdot \vec{\xi} \quad , \end{aligned}$$

and

$$\begin{aligned} -L_{AA} &= -2J_{AA} \{ \cos \vec{k} \cdot (\vec{\xi} + \vec{\eta} + \vec{\xi}) + \cos \vec{k} \cdot (\vec{\xi} - \vec{\eta} - \vec{\xi}) + \cos \vec{k} \cdot (-\vec{\xi} + \vec{\eta} - \vec{\xi}) \\ &\quad + \cos \vec{k} \cdot (-\vec{\xi} - \vec{\eta} + \vec{\xi}) \} - 2J'_{AA} \cos (2\vec{k} \cdot \vec{\eta}) \quad . \end{aligned}$$

Let

$$\begin{aligned} x &\equiv \cos \vec{k} \cdot \vec{\xi} \quad , \quad y \equiv \cos \vec{k} \cdot \vec{\eta} \quad , \quad z \equiv \vec{k} \cdot \vec{\xi} \quad , \\ q &\equiv J'_{AB}/J_{AB} = 1 + \alpha > 1 \quad , \quad q' \equiv J_{AA}/J_{AB} \quad , \quad q'' = J'_{AA}/J_{AB} \quad . \end{aligned} \quad (C-15)$$

Then from (C-14) the problem is to maximize $f(\vec{k})$, where

$$f(\vec{k}) \equiv \lambda/4J_{AB} = (y^2 + q^2 z^2 + 2qxyz)^{1/2} - 4q'xyz - q''(2y^2 - 1) \quad . \quad (C-16)$$

This problem has several solutions:

Case 1: $\sin \vec{k} \cdot \vec{\xi} = \sin \vec{k} \cdot \vec{\eta} = \sin \vec{k} \cdot \vec{\xi} = 0$, and $xyz > 0$. Here $x = \pm 1$, $y = \pm 1$, $z = \pm 1$ and $f(1, 1, 1) = f(1, \bar{1}, \bar{1}) = f(\bar{1}, 1, \bar{1}) = f(\bar{1}, \bar{1}, 1)$. This does not represent a real degeneracy, however. Consider $(1, 1, 1)$. Here

$$\vec{k} \cdot \vec{\eta} = 0 \quad , \quad \vec{k} \cdot \vec{\xi} = \vec{k} \cdot \vec{\xi} = \pi \quad , \quad \text{and} \quad \vec{k} \cdot \vec{R}_{\ell mn} = \vec{k} \cdot (\ell \vec{\xi} + m \vec{\eta} + n \vec{\xi}) = 2\pi$$

since $\ell = n = 1$ on going to a near neighbor. Thus near-neighbor interactions are ferromagnetic. For Case 1,

$$f(1, 1, 1) = 1 + q - 4q' - q'' \quad . \quad (C-17)$$

Case 2: $x = \pm 1$, $y = \pm 1$, $z = \pm 1$, and $xyz < 0$. In this case,

$$f(\bar{1}, 1, 1) = \alpha + 4q' - q'' \quad ,$$

where the following parametric definitions hold:

$$\alpha \equiv q - 1 \quad , \quad \beta \equiv q/4q' = J'_{AB}/4J_{AA} \quad , \quad \gamma \equiv qq''/2q' = J'_{AB}J'_{AA}/2J_{AB}J_{AA} \quad . \quad (C-18)$$

Case 3: $x = \pm 1$, $y = \pm 1$, $z = \pm 1/q$, and $xyz > 0$.

$$f(1, 1, 1/q) = 2 - \beta^{-1} - q'' \quad . \quad (C-19)$$

Case 4: $x = \pm 1$, $y = \pm 1$, $z = \pm 1/q$, and $xyz < 0$.

$$f(1, 1, 1/q) = \beta^{-1}(1 - \gamma) + q'' \quad . \quad (C-20)$$

Case 5: $x = \pm 1$, $y = \pm \beta$, $z = \pm(\beta/q)(1 + 2\gamma)$, and $xyz < 0$.

$$f[1, \beta, (-\beta/q)(1 + 2\gamma)] = \beta(1 + 3\gamma) + q'' \quad . \quad (C-21)$$

Case 6: $x = 0$, $y = \pm 1$, and $z = 0$.

$$f(0, 1, 0) = 1 - q'' \quad . \quad (C-22)$$

Case 7: $x = \pm(1 + q^2 - \beta^2)/2q$, $y = \pm 1$, $z = \pm 1$, and $xyz > 0$.

$$f[(1 + q^2 - \beta^2)/2q, 1, 1] = (2 + 2q^2 - \beta^2)^{1/2} - (1 + q^2 - \beta^2)/2\beta - q'' \quad . \quad (C-23)$$

Case 8: $x = \pm(1 + q^2 - \beta^2)/2q$, $y = \pm 1$, $z = \pm 1$, and $xyz < 0$.

$$f[(1 + q^2 - \beta^2)/2q, 1, \bar{1}] = (1 + q^2 + \beta^2)/2\beta - q'' \quad . \quad (C-24)$$

Case 9: $-1 \leq x \leq 1$, $y = 0$, $z = \pm 1$.

$$f(x, 0, 1) = q + q'' \quad (C-25)$$

Case 10: $x = \pm y(1 + 2\gamma)/2q$, $y^2 = (q^2 - \beta^2)/2\gamma < 1$, $z = \pm 1$, and $xyz < 0$.

$$f[y(1 + 2\gamma)/2q, y, \bar{1}] = \beta + q'' + (q^2 - \beta^2)/4\beta\gamma \quad . \quad (C-26)$$

Case 11: $x = \pm 1$, $y = |\beta - q|/2\gamma$, $z = \pm 1$, and $xz > 0$.

$$f(1, |\beta - q|/2\gamma, 1) = q + q'' + (\beta - q)^2/4\beta\gamma \quad (C-27)$$

Case 12: $x = \pm 1$, $y = (\beta + q)/2\gamma$, $z = \pm 1$, and $xz < 0$.

$$f[1, (\beta + q)/2\gamma, \bar{1}] = q + q'' + (\beta + q)(\beta - 3q)/4\beta\gamma \quad (C-28)$$

Case 13: $x = x$, $y = z = 0$.

$$f(x, 0, 0) = q'' \quad . \quad (C-29)$$

Case 14: $x = x$, $y = \beta$, $z = 0$.

$$f(x, \beta, 0) = \beta(1 - \gamma) + q'' \quad . \quad (C-30)$$

Case 15: $x = \pm \frac{1}{2}(1 + 2\gamma)^{1/2}$, $y = \pm\beta$, $z = \pm\beta(1 + 2\gamma)^{1/2}/q$, and $xyz < 0$.

$$f[\frac{1}{2}(1 + 2\gamma)^{1/2}, \beta, -\beta(1 + 2\gamma)^{1/2}/q] = \frac{3}{2}\beta + q'' \quad . \quad (C-31)$$

In the case of MnP, it is estimated that $0 \leq \alpha \leq 1/2$. Therefore, Fig. 8 shows the magnetic phase diagram, obtained by maximizing $f(\vec{k})$ from Eqs. (C-17) through (C-31), for $\alpha = 0$ and $\alpha = 1/2$.

If $J'_{AA} = J'_{AA}(T)$ increases with decreasing temperature and the other exchange parameters are relatively insensitive to temperature, the γ increases with decreasing temperature. Therefore, any antiferromagnetic \rightleftharpoons ferromagnetic transition as a function of temperature indicates that the antiferromagnetic phase corresponds to Case 11. Case 11 corresponds to a flat spiral propagating along the orthorhombic c-axis. Orthorhombic (001) planes are ferromagnetic, and the turn angle between successive (001) planes is Θ_o , where

$$\cos \Theta_o = (\beta - q)/2\gamma = (J_{AB} - 4J_{AA})/4J'_{AA} \quad . \quad (C-32)$$

The plane in which the spins lie is determined by the crystalline anisotropy. It need not lie perpendicular to the \vec{k} vector. For a hard a-axis, the spins lie in the b-c plane.

Since spins within (001) planes remain parallel in the presence of external and anisotropy fields, Eq. (C-32) shows that calculation of low-field susceptibilities and of the critical field H_k

for a spiral $\vec{\tau}$ ferromagnetic transformation can be done via a simpler problem, viz., one where (001) planes couple ferromagnetically to near-neighbor (001) planes by an effective exchange parameter $J = (J_{AB} - 4J_{AA})$ and antiferromagnetically to next-near-neighbor (001) planes by $J_2 = -J'_{AA}(1 - \alpha_s \epsilon_n)$, where $\epsilon_n = [(\vec{R}_{n+2} - \vec{R}_n) - (\vec{R}_{0,n+2} - \vec{R}_{0,n})]/2\eta$ is the strain induced by exchange striction, and α_s is a nondimensional parameter. The factor $(1 - \alpha_s \epsilon_n)$ must be introduced if the magnitude of J'_{AA} is sufficiently sensitive to the cation-cation separation 2η that its variation with temperature can induce an antiferromagnetic $\vec{\tau}$ ferromagnetic transition. If φ_n is the angle the moment of the n^{th} (001) plane makes with the direction of an \vec{H} applied,

$$\begin{aligned} E_{\text{ex}} &= -M_s^2 \sum_n [J \cos(\varphi_{n+1} - \varphi_n) - J'_{AA}(1 - \alpha_s \epsilon_n) \cos(\varphi_{n+2} - \varphi_n)] \quad , \\ E_K &= \sum_n K \sin^2(\varphi_n - \varphi_H) \quad , \\ E_H &= -\sum_n H M_s \cos \varphi_n \quad , \\ E_{\text{el}} &= \sum_n Y \epsilon_n^2 \quad , \end{aligned} \tag{C-33}$$

where φ_H is the angle between the applied field H and the c -axis and Y is Young's modulus. Minimization of the total energy with respect to ϵ_n gives

$$\epsilon_n = \epsilon_0 \cos(\varphi_{n+2} - \varphi_n) \quad , \tag{C-34}$$

where $\epsilon_0 = \alpha_s J'_{AA} M_s^2 / 2Y$. If $H = K = 0$, the magnetic spiral remains simple and the exchange striction is uniform. In this case,

$$\varphi_n(H = K = 0) \equiv \varphi_n^0 = n\Theta \quad , \tag{C-35}$$

and minimization of E_{ex} with respect to Θ yields

$$\cos \Theta (1 - 2\alpha_s \epsilon_0 \cos 2\Theta) = J/4J'_{AA} = (J_{AB} - 4J_{AA})/4J'_{AA} \quad . \tag{C-36}$$

For $\alpha_s \epsilon_0 \ll 1$, this reduces to

$$\cos \Theta \approx \cos \Theta_0 [1 + 2\alpha_s \epsilon_0 (2 \cos^2 \Theta_0 - 1)] \quad , \tag{C-37}$$

where Θ_0 is defined by Eq. (C-32). Thus, if $\Theta_0 > \pi/4$, exchange striction increases the turn angle ($\Theta > \Theta_0$), and if $\Theta_0 < \pi/4$, it decreases the turn angle ($\Theta < \Theta_0$).

If $H \ll M_s J$ and $k \ll M_s^2 J$, it is possible to use perturbation theory, and

$$\varphi_n = \varphi_n^0 + \psi_n = n\Theta + \psi_n \quad . \tag{C-38}$$

Since $(\psi_{n+j} - \psi_n) \ll 1$, there are the relations:

$$\begin{aligned} \sin(\varphi_{n+j} - \varphi_n) - \sin(\varphi_n - \varphi_{n-j}) &\approx \cos(j\Theta) (\psi_{n+j} - 2\psi_n + \psi_{n-j}) \quad , \\ \frac{1}{2} [\sin 2(\varphi_{n+j} - \varphi_n) - \sin 2(\varphi_n - \varphi_{n-j})] &\approx \cos(2j\Theta) (\psi_{n+j} - 2\psi_n + \psi_{n-j}) \quad . \end{aligned}$$

Substitution of these relations into the condition $\partial E / \partial \varphi_n = 0$ gives

$$\begin{aligned} (H/M_S) \sin(n\theta) + (\epsilon K/M_S^2) \sin(2n\theta) &= J \cos \theta (\psi_{n+1} - 2\psi_n + \psi_{n-1}) \\ &\quad - J'_{AA} (\cos 2\theta - \alpha_S \epsilon_O \cos 4\theta) (\psi_{n+2} - 2\psi_n + \psi_{n-2}) \quad , \end{aligned}$$

where

$$\epsilon = +1 \quad \text{if} \quad \vec{H} \parallel \vec{c} \quad , \quad \epsilon = -1 \quad \text{if} \quad \vec{H} \parallel \vec{b} \quad . \quad (\text{C-39})$$

Now let

$$\psi_n = E e^{i\nu n} + E' e^{-i\nu' n} + \text{c.c.} \quad , \quad (\text{C-40})$$

and solutions are obtained if

$$E = e/2i = e^*/2i \quad , \quad E' = e'/2i = e'^*/2i \quad , \quad \nu = \theta \quad , \quad \nu' = 2\theta \quad .$$

If Eq. (C-36) is also used, Eq. (C-38) becomes

$$\varphi_n = n\theta - \epsilon h_A \sin(2n\theta) - h \sin(n\theta) \quad , \quad (\text{C-41})$$

where

$$\begin{aligned} h_A &\equiv (2K/M_S^2) / \{ 64J'_{AA} \Theta^4 [1 - \frac{1}{2} (\alpha_S \epsilon_O / \Theta^2) - \frac{4}{3} \alpha_S \epsilon_O] \} \quad , \\ h &\equiv (H/M_S) / \{ 5J'_{AA} \Theta^4 [1 - \frac{4}{5} (\alpha_S \epsilon_O / \Theta^2) - \frac{26}{15} \alpha_S \epsilon_O] \} \quad . \end{aligned}$$

For $K = \alpha = 0$, this solution reduces to that derived by Enz³² via a continuum model.

The critical field H_k is obtained by setting the total energy of spiral (11) with $H = 0$ equal to the total energy for the ferromagnetic phase $H = H_k$. This gives

$$H_k/M_S = \frac{1}{2} J'_{AA} \Theta^4 [1 + 2(\alpha_S \epsilon_O / \Theta^2) - \frac{32}{3} \alpha_S \epsilon_O] + (K/M_S^2) (\sin^2 \varphi_H - \frac{1}{2} + \frac{1}{2} \epsilon h_A) \quad . \quad (\text{C-42})$$

If $\vec{H} \parallel \vec{c}$, $\varphi_H = 0$ and $\epsilon = +1$; if $\vec{H} \parallel \vec{b}$, $\varphi_H \rightarrow \pi/2$ and $\epsilon = -1$. Therefore, the difference in H_k for $\vec{H} \parallel \vec{b}$ and $\vec{H} \parallel \vec{c}$ is

$$H_{kb} - H_{kc} = (K/M_S) - h_A M_S \quad . \quad (\text{C-43})$$

The magnetic moment is given by

$$M/M_S = \langle \cos \varphi_n \rangle \approx \frac{1}{2} h (1 - \frac{1}{2} \epsilon h_A) \quad ,$$

so that the magnetic susceptibility is

$$\chi = M/H = (1 - \frac{1}{2} \epsilon h_A) / \{ 10J'_{AA} \Theta^4 [1 - \frac{4}{5} (\alpha_S \epsilon_O / \Theta^2) - \frac{26}{15} \alpha_S \epsilon_O] \} \quad , \quad (\text{C-44})$$

and

$$\chi_c - \chi_b = -\frac{1}{2} h_A (\chi_c + \chi_b) = -\frac{1}{6.4} \left(\frac{2K}{M_S^2} \right) \left(\frac{\chi_c + \chi_b}{2} \right)^2 \left[\frac{1 - \frac{4}{5} (\alpha_S \epsilon_O / \Theta^2) - \frac{26}{15} \alpha_S \epsilon_O}{1 - \frac{1}{2} (\alpha_S \epsilon_O / \Theta^2) - \frac{4}{3} \alpha_S \epsilon_O} \right] \quad . \quad (\text{C-45})$$

There are two contributions to the total anisotropy constant K , a purely crystalline term K_c and a dipole-dipole term K_d . Huber and Ridgley⁵ report a $2K/M_S^2 = 40$ for the ferromagnetic

phase just above the transition. The dipole-dipole term arises from the fact that large crystalline anisotropy ($K_1 = 1.4 \times 10^7$ ergs/cm³ is the anisotropy constant for the a-c plane in the ferromagnetic phase⁵) forces the plane of the spiral to be parallel to the propagation direction for the spiral. In this configuration, the component of the magnetization along the propagation direction (c-axis) changes sign every half wavelength, so that within each half wavelength there are demagnetizing fields equivalent to $8\pi M'$, where the magnetization is roughly $M' = M_s \langle \sin \theta \rangle_0^\pi = 2M_s/\pi$. Therefore, $-2K_d/M_s^2 \approx 16$. If the crystalline anisotropy of the ferromagnetic phase is extrapolated into the antiferromagnetic phase, it follows that in the antiferromagnetic phase

$$2K/M_s^2 \approx 20 \quad . \quad (C-46)$$

It should be noted that the large K_d tends to stabilize simple spirals into a configuration in which the plane of the spiral is perpendicular to the propagation vector \vec{k} . It is only in the presence of large crystalline anisotropies that the plane of the spiral can contain the propagation vector to give a "cycloidal" spiral.

Experimentally,⁵ $(1/2)(\chi_c + \chi_b) \approx 5 \times 10^{-3}$ emu/cm³-oe. Therefore, if $2\epsilon_0 = 0$, Eqs. (C-45) and (C-46) give

$$\chi_c - \chi_b \approx -10^{-4} \text{ emu/cm}^3\text{-oe} \quad ,$$

which is at least an order of magnitude smaller and of opposite sign than the measured⁵ $(\chi_c - \chi_b)_{\text{expt}} \approx 2.5 \times 10^{-3}$ emu/cm³-oe. Therefore, it appears that exchange striction plays an important role. In order to obtain both the correct sign and magnitude for $\chi_c - \chi_b$, it is necessary to have

$$(1 - \frac{4}{3} \alpha_s \epsilon_0) > \frac{1}{2} (\alpha_s \epsilon_0 / \theta^2) \quad , \quad (1 - \frac{26}{15} \alpha_s \epsilon_0) < \frac{4}{5} (\alpha_s \epsilon_0 / \theta^2) \quad ,$$

and

$$1 - \frac{4}{3} \alpha_s \epsilon_0 \approx \frac{1}{2} (\alpha_s \epsilon_0 / \theta^2) \quad .$$

Given a $\theta = \pi/9 = 20^\circ$, the last requirement leads to an $\alpha \sim 15$ and $\epsilon_0 \sim 0.015$ if $\alpha_s \epsilon_0 \sim \alpha_s^2 10^{-2}$. These numbers are reasonable. They lead to the prediction of a measurable modulation of the c-axis spacing that has half the wavelength of the spiral. This prediction can be checked by a combination of neutron-diffraction and x-ray diffraction experiments.

REFERENCES

1. J. B. Goodenough, Phys. Rev. 117, 1442 (1960).
2. J. B. Goodenough, Phys. Rev. 120, 67 (1960).
3. D. H. Lyons and T. A. Koplon, Phys. Rev. 120, 1580 (1960); T. A. Koplon, K. Dwight, D. H. Lyons and N. Menyuk, J. Appl. Phys. Suppl. 32, 135 (1961).
4. P. W. Anderson, Phys. Rev. 115, 2 (1959).
5. E. E. Huber, Jr. and D. H. Ridgley, J. Appl. Phys. 34, 1099 (1963); Phys. Rev. (to be published).
6. R. K. Nesbet, Phys. Rev. 122, 1497 (1961) and to be published.
7. M. A. Ruderman and C. Kittel, Phys. Rev. 96, 99 (1954).
8. T. Kosuyo, Prog. Theoret. Phys. (Kyoto) 16, 45 (1956); K. Yosida, Phys. Rev. 106, 893 (1957).
9. N. F. Mott, Con. J. Phys. 34, 1356 (1956); Nuovo cimento [10] 7, Suppl., 312 (1958).
10. G. H. Jonker and S. Van Houten, "Semiconducting Properties of Transition Metal Oxides" in Holbleiter probleme VI, F. Souter, Ed. (Friedr. Vieweg und Sohn, Braunschweig, 1961), p. 118.
11. T. Holstein, Ann. Phys. (N. Y.) 8, 325, 343 (1959).
12. J. H. Von Sonten and J. S. Von Wierengen, Rec. trav. chim. (Pays-Bas) 71, 420 (1952).
13. S. Foner, Phys. Rev. 107, 683 (1957); J. phys. radium 20, 336 (1959).
14. S. Foner, Phys. Rev. (to be published).
15. L. M. Corliss and J. M. Hastings (private communication).
16. J. C. Gill, Nature 100, 619 (1961); H. Stotz, M. J. Weber, L. Rimoi, G. A. de Mors and G. F. Koster, J. Phys. Soc. Japon 17, Suppl. B-1, 430 (1962).
17. E. Thilo, J. Jander and H. Seeman, Z. anorg. u. allgem. Chem. 279, 2 (1955).
18. G. W. Prott, Jr. and P. T. Bailey, Phys. Rev. (to be published).
19. S. C. Abrahams, Phys. Rev. (to be published).
20. F. J. Morin, Phys. Rev. Letters 3, 34 (1959).
21. M. Foëx and J. Wucher, Compt. rend. 241, 184 (1955); A. D. Pearson, J. Phys. Chem. Solids 5, 316 (1958).
22. R. E. Newnham and Y. M. de Hoon, Quarterly Progress Report XXVI, Laboratory for Insulation Research, M. I. T. (January 1960), p. 10; Z. Krist. 117, 235 (1962).
23. D. B. Rogers, A. Wold, R. J. Arnett and J. B. Goodenough, J. Phys. Chem. Solids 24, 34 (1963).
24. J. B. Goodenough, J. Appl. Phys. Suppl. 33, 1197 (1962).
25. H. Wotonobe, H. Yomomoto and K. Ito, J. Phys. Soc. Japon 18, 995 (1963).
26. Y. Tonobe and S. Sugono, J. Phys. Soc. Japon 9, 753 (1954).
27. C. K. Jorgensen, Absorption Spectro and Chemical Bonding in Complexes (Pergamon Press, London, 1962), p. 285 and Chap. 7.
28. A. J. P. Meyer and M. C. Codeville, J. Phys. Soc. Japon 17, Suppl. B-1, 223 (1962).
29. C. J. Kriessman and H. B. Collen, Phys. Rev. 94, 837 (1954).
30. R. Benoit, J. Chim. Phys. 52, 119 (1955).
31. J. M. Luttinger and L. Tisza, Phys. Rev. 70, 954 (1946).
32. U.ENZ, J. Appl. Phys. Suppl. 32, 225 (1961).